Polyphase Deformation and Strain Migration on the Septentrional-Oriente Fault Zone in the Windward Passage, Northern Caribbean Plate Boundary

A. Oliveira de Sá, Elia d'Acremont, Sylvie Leroy, Sara Lafuerza

Polyphase deformation and strain migration on the Septentrional-Oriente Fault Zone in the Windward Passage, Northern Caribbean Plate boundary

A. Oliveira de Sá[1], E. d'Acremont[1], S. Leroy[1], and S. Lafuerza[1]

[1] Sorbonne Université, CNRS-INSU, Institut des Sciences de la Terre Paris, ISTeP, 75005 Paris, France

Corresponding author: Alana Oliveira de Sá (alana.oliveira_de_sa@sorbonne-universite.fr)

Key Points:

- The present-day structure in the Windward Passage implies a polyphase evolution with at least 4 stages of deformation.
- Motion on the Septentrional-Oriente Fault in the Windward Passage began in early Pliocene time and has generated an estimated ~80 km offset
- Onset of motion in the Windward Passage is key to revealing Neogene structural evolution of the northern Caribbean plate.

Keywords: Windward Passage, Septentrional-Oriente Fault Zone, Northern Caribbean plate, strain migration, strike-slip faults, Hispaniola

Abstract

Oblique collision between the Caribbean plate and the Bahama Banks has lead an eastward migration of the northern Caribbean plate boundary by successive southward jumps of major strike-slip faults. The Septentrional-Oriente Fault zone (SOFZ) defines the present-day northern Caribbean plate boundary accommodating most of the eastward escape of the Caribbean plate. Here, we reevaluate the complex history of the SOFZ along the Windward Passage area between the easternmost region of Cuba and the northwest of Haiti. Based on seismic reflection and swath-bathymetric dataset we interpret the structure and tectonic pattern of the Windward Passage. The tectono-sedimentary framework of this large strait shows contrasting patterns of deformation linked to a complex polyphase tectonic history of dominantly strike-slip faulting. SOFZ segments offset the seismic units and yield key markers of displacement along the fault system. Our study provides structural and stratigraphic insights into the relative timing of deformation along the Windward Passage and presents new elements that constrain the southeastward jump of the north Caribbean plate boundary to its present-day position. We propose dates for the identified seismic units based on the correlation of offshore deformation phases recorded in the Windward Passage sedimentary cover with major paleogeographic reorganization episodes described onland (Late Eocene, Late Oligocene, Middle Miocene and Late Pliocene). By restoring the offset of the seismic units, we demonstrate that at least ~80 km of left-lateral motion has occurred on the SOFZ, and that the SOFZ has been active since the Pliocene.

1 Introduction

Relative plate motion at most convergent plate boundaries is oblique to the boundary itself (Philippon & Corti, 2016). Oblique convergence settings display strain partitioning into boundary-normal and boundary-parallel components of the plate motion vector (Jarrard, 1986; Demets, 1992; ten Brink & Lin, 2004; Chemenda et al., 2000). In oblique convergence settings, the oblique component of motion is often accommodated by strike-slip faults that dominate plate interactions (Teyssier et al., 1995; Chemenda et al., 2000). In such cases, strike-slip faults may also form along the edge of the overriding plate to accommodate boundary-parallel components (Fitch, 1972; Jarrard, 1986). This process is called slip partitioning and it has been observed in oblique convergence contexts such as offshore Sumatra (Jarrard, 1986), the Philippine fault (Fitch, 1972), in Taiwan (Lallemand et al., 1999) and in the Lesser Antilles (Symithe et al., 2015; Laurencin et al., 2019). Along the Caribbean–North American plate boundary, the degree of obliquity varies from ~50° North of Cuba, ~20° in the northern Hispaniola Island arc, to up to 72° in the northern Lesser Antilles (Calais et al. 2016; Laurencin et al., 2019; Rodríguez-Zurrunero et al., 2020). To the north of Hispaniola, the eastward motion of the Caribbean Plate is slowed by its collision with the Bahama Banks. Caribbean plate motion is highly oblique to this portion of the plate boundary (Figure 1)(Demets, 1992; Mullins et al., 1992; Calais et al., 2016). This ongoing oblique collision result in a strong stress coupling between the plates and slip partitioning along the northern edge of Hispaniola (Rodríguez-Zurrunero et al., 2020). North-verging fold propagation faults sub-parallel to the Caribbean plate displacement accommodates part of the convergence in Hispanolia's northern coast (Calais et al., 2010). Oblique motion is also accommodated by a large-scale, seismically active strike-slip fault system, known as the Septentrional-Oriente Fault Zone (SOFZ), which forms the current northern Caribbean Plate boundary (Leroy et al., 2015; Calais et al., 2016)(Figure 1).

The SOFZ trends almost E-W as it runs along the southern coast of Cuban, and straight across the Windward Passage until it steps onland in northern Hispaniola (Figure 1a). The geological setting of the region has been strongly controlled by this large-scale strike-slip fault system (de Zoeten & Mann, 1991; Mann et al., 1995; Rojas-Agramonte et al., 2008). Previous seismic reflection data has led to an initial description of the SOFZ and its related structural framework (Calais & Mercier de Lépinay, 1991; Dillon et al., 1992; Calais & Mercier de Lépinay, 1995; Leroy et al., 2015). However, the initiation of SOFZ remains poorly constrained, as well as the understanding of how the various segments of the system may have functioned as the convergent plate boundary evolved.

This paper documents the sedimentary and structural framework associated with the active segments of the SOFZ in the Windward Passage. The study area is located at the contact zone between the North American Plate and the northern boundary of the Caribbean Plate. The Windward Passage may have recorded a wealth of information concerning tectonic events at the Caribbean–North American plate boundary. It is thus a critical witness to the kinematic evolution of the Caribbean Plate.

The main goal of this study is to understand how the tectonic context of oblique collision with strain partitioning within the Windward Passage since the Eocene has led to the current sedimentary and structural framework. We present high-resolution multibeam bathymetry and ~3000 km of multi-channel seismic reflection profiles that image the Windward Passage domains, mapping the SOFZ fault trace and related morphological features (Figure 2). Deformation events recorded in the sedimentary cover were time-correlated with major onland

deformation events in southern Cuba and Northern Hispaniola. Our intent is to (i) constrain the deformation styles in time through interpretation of the sedimentary record, (ii) infer the structural framework that existed prior to inception of the SOFZ, and (iii) better understand the current structures associated to this major fault system. We discuss the critical time markers for inferring the stratigraphic interval that defines a timeframe for the initiation of left-lateral strike-slip motion on the SOFZ within the Windward Passage and its subsequent migration. We accurately define the active tectonics of the Northern Caribbean plate boundary, providing a better understanding of the regional tectonics.

2 Tectonic Settings

Since Paleocene times, the Caribbean–North American plate boundary has undergone progressive reorganization in response to the diachronous collision between the Cuban-Hispaniola Arc and the Bahama Banks (Gordon et al., 1997; Iturralde-Vinent & Macphee, 1999; Mann et al., 2002). This collision has caused a change in the Caribbean-North American relative plate motion from NNE to E (Pindell et al., 2005; Boschman et al., 2014). Along the Cuban Arc, strain partitioning and large-scale strike-slip faulting took place. The northern Caribbean plate boundary underwent a series of jumps. During the initial stages of collision, the boundary coincided with the eastern Yucatan transform margin. Accommodation of relative plate motion migrated progressively southward as each new fault systems developed and was subsequently replace by a younger fault system starting with the development of the Pinar fault (Paleocene), followed by the La Trocha fault (Early Eocene), and then the Cauto fault (middle Eocene) in Cuba (Figures 3a and 3b). As the plate boundary shifted southward to the Oriente Fault zone (OFZ) (early Oligocene), the Cuban block became attached to the North American Plate resulting in the separation of Cuba and Hispaniola, which until then had formed a single block (Figure 3c)(Calais & Mercier de Lépinay, 1992; Leroy et al., 2000; Rojas-Agramonte et al., 2008; Wessels, 2019). The OFZ transcurrent plate boundary must have been located north of Hispaniola during the Miocene until Pliocene times (Figures 3d, 3e and 3f)(Erikson et al., 1998). However, as the system evolved the northern end of the OFZ gradually became inactive and the strike-slip motion between Cuba and Hispaniola shifted southward (Calais & Mercier de Lépinay, 1995), extending into the northwestern peninsula of Hispaniola to form the Septentrional fault (Late Pliocene) and establish the current Septentrional-Oriente Fault Zone (SOFZ) (Figures 1b, 3f and 3g) (Calais et al., 2016; Escuder-Viruete and Pérez, 2020).

On the Island of Hispaniola, the SOFZ and the North Hispaniola fault (Deformation front) partition the oblique convergence into boundary-parallel and boundary-normal components (Rodríguez-Zurrunero et al., 2019, 2020). The SOFZ accommodates most of the left-lateral strain of the current Caribbean-North American relative plate motion as a major transpressional fault system. Using GPS measurements and block modelling, Calais et al. (2010) estimate that the SOFZ currently accumulates elastic strain at a rate of 12 ± 3 mm yr^{-1}. While the North Hispaniola fault accommodates 2 to 6 mm/yr of ~N-S shortening, and the Trans-Haitian belt accommodates about 4 mm $yr^{-1}$of ~N-S shortening (Figure 1a).

The Windward Passage area is a large strait separating the eastern extremity of Cuba from the northwestern peninsula of Hispaniola (Figure 1b) (Calais, 1990). The area consists of a submarine plateau, the Windward Passage Sill (WPS) (Goreau, 1989) and an adjacent sedimentary basin, the Windward Passage Deep (WPD) (Calais & Mercier de Lépinay, 1995). A

forward-propagating imbricated zone of contractional structures characterizes the WPS on its northern edge and delimits the deformation front (Figure 2)(Goreau, 1989; Dillon et al., 1992, 1996; Rodríguez-Zurrunero et al., 2019). There, sediments of the adjacent Hispaniola basin are tilted to the north and incorporated into the WPS structure. To the south, the WPS is bounded by the WPD, an east-west trending elongated basin. The WPD is about 120 km long and 15 km wide with depths ranging from 1100 to 3780 m (Figure 2a). The evolution of the WPD is interwoven with SOFZ formation, which crosses its entire length running from the southern Cuban margin eastward to the northern Hispaniola margin (Figure 2b). Calais & Mercier de Lépinay (1995) correlate offshore seismic sequences recognized in the WPD to successive tectonic and sedimentary events recorded onshore in Cuba and Hispaniola. These authors associate these correlated onshore-offshore events with the successive collisions of the northern Caribbean mobile terranes against the Bahama Bank.

3 Data and Methods

Multichannel seismic reflection and multibeam bathymetric data were collected during cruises HAITI-SIS 1-2 (2012-2013) onboard the R/V L'Atalante from the Flotte Océanographique Française (Leroy, 2012; Leroy and Ellouz-Zimmermann, 2013; Leroy et al., 2015). Multibeam bathymetric data collected during NORCARIBE geophysical cruise in November–December 2013 aboard the Spanish R/V Sarmiento de Gamboa is used to fill the gaps in our data coverage (Leroy et al 2015; Rodríguez-Zurrunero et al., 2020). In this paper, we focus on the Windward Passage area where ~3000 km of seismic profiles have been acquired (Figure 1b). Seismic reflection data are recorded using a source comprising two GI air guns (2.46 L, 300 in3) and a streamer with 24 traces (600 m long) operated at c.a 9.7 knots (fast and light seismic system). The multichannel seismic reflection data were processed using classical steps including CDP gathering (fold 6), binning at 25m, detailed velocity analysis, stack and post-stack time migration. All the seismic reflection profiles presented are time migrated. Multibeam bathymetry data were acquired simultaneously along seismic profiles and gridded with a spacing of 50 m. The gridded bathymetry data was augmented with the GEBCO Digital Atlas (https://www.gebco.net/data_and_products/gebco_digital_atlas/) with an 800m resolution to provide an almost full coverage (Figure 1a). The processed seismic data are interpreted using Kingdom IHS Suite© software. Maps are plotted with ArcGIS© software. We use the seismic reflection dataset to identify sedimentary units, deformation style and spatio-temporal evolution of the tectonic structures. Morphological analysis of the seafloor based on swath-bathymetric data is carried out to identify the surface signature of tectonic features (Figure 2). We identify faults by either sediment horizon offsets or by the fault plane seismic reflection itself in the available seismic profiles.

4 Results

4.1 Seismic stratigraphy

Seismic units are hereafter described by geographic sectors and ordered from the acoustic basement to the most recent one (Unit 4). We summarize the corresponding facies in a table (Figure 4). For both areas, WPS and WPD, the top of the acoustic basement corresponds to a rough surface on some profiles (Figures 5, 6 and 7), and it may outcrop in the structural highs of the study area (Figure 5, km 40-55). Acoustic energy is insufficient to image beneath the top of the observed acoustic basement (labelled unconformity Uc1). The presence of seabed multiples

usually hampers the description of internal geometry of the acoustic basement. When seismic reflections are observed within the acoustic basement, the reflectors are discontinuous to chaotic, medium-high amplitudes that may terminate upward against the irregular and rugged unconformity Uc1 (Figures 4, 5 and 6).

4.1.1 Windward Passage Sill

Within the Windward Passage Sill (WPS), we define three main seismic units above the acoustic basement that correspond to seismic units previously defined by Calais and Mercier de Lépinay (1995). The lower unit (Unit 1) is characterized by a thick series (>1s TWT) with at least two internal angular unconformities (Uc1a and Uc1b, Figures 6 and 7) that separate distinct sub-units of distinct facies and geometries (Units 1a, 1b and 1c; see Figure 4 for detailed reflections attributes).

At the base of Unit 1, the seismic facies is transparent (Unit 1a in Figures 4 and 7, km 65-85), then well-defined by parallel high frequency reflections in its upper part (Unit 1c, Figure 4). Most of Unit 1, especially its base, appears to have been folded and then eroded as indicated by unconformities Uc1a and Uc1b (Figure 7, km 65-85). In the northern flank of the WPS high, Units 1a and 1b onlap the angular unconformity Uc1 (Figure 6, km 33-43) and Unit 2 is not present. The second seismic unit in the WPS (Unit 3) is separated from the Unit 1 by an angular unconformity labelled Uc3 (Figures 4 and 6). Unit 3 layers are tilted and folded and were deposited in the syncline depressions formed by the previous folding of Unit 1, with a succession of onlap terminations in a well-layered sequence (Figure 6, km 25-40).

The angular unconformity Uc4 is observed at the top of Unit 3 and separates Unit 3 from the more horizontally layered high-frequency reflectors of uppermost Unit 4 (Figures 4 and 6). Our seismic profiles through the WPS illustrate the lateral thickness variation of Unit 4. The thickness of this unit increases from north to south (Figure 6, km 40-20) and more clearly from west to east: increasing from 160 m in the western part (conversion of 0.2 s TWT by using a P-wave velocity of 1600 m/s for less consolidated sediments; Figure 7) to up to 480 m in its eastern part near the Tortue Island (Figures 6 and 8d).

Toward the east, close to Tortue Island, the seismic profiles display an unconformity that truncates the horizontally stratified, undisturbed reflectors of Unit 4 (unconformity Uc4a in Figures 8b and 8c). Unit 4 is therefore subdivided into two sub-units: Unit 4a that shows parallel high frequency reflectors and Unit 4b with parallel moderate frequency, low-amplitude reflectors interspersed with thin chaotic beds (see Figure 4). The thickness of Unit 4b varies from north to south (Figures 8a and 8b) and from west to east (Figures 8c and 8d). On the northern slope off Tortue Island its thickness reaches 0.6 s TWT (~480m thick)(Figure 8d, km 25-30). Westward, this sub-unit is almost completely eroded (Figures 6 and 8c). Recent mass wasting processes probably affected the shape of the slope in the WPS area, eroding the upmost part of Unit 4b.

4.1.2 Windward Passage Deep

Sedimentary units in the WPD area do not show clear correlations with those found in the WPS. Units 1 and 4 are common to both areas (Figures 4 and 6). However, in the WPD these units show some slightly differences in their facies (Figure 4):

As observed in the WPS area, Unit 1 consists of parallel to sub-parallel high-amplitude and low-frequency reflections onlapping the basement in the WPD area (Figure 6). Punctually,

its seismic facies become transparent to chaotic and the unit displays lateral variations of thickness (Figure 4). Its bottom geometry is barely visible on seismic data. In the WPD area the Unit 1 does not clearly display distinct sub-units as described in the WPS area.

Unit 2 is a distinct sedimentary unit present only in the WPD area (Figures 6, 7 and 9). It overlies Unit 1 on the angular unconformity Uc2 (Figure 10). Its thickness and internal reflection pattern vary throughout the basin. In the north wall of the WPD (southern flank of the WPS), Unit 2 is perched (Figure 5). Unit 2 is thus defined by parallel to sub-parallel continuous reflectors, which are onlapping the steeply dipping Uc1 unconformity at its northern boundary (Figure 5, km 25-40). Its thickness is about 1.2s TWT (~960m thick; conversion of 1.2 s TWT by using a P-wave velocity of 1600 m/s for less consolidated sediments), and it thickens slightly northward (Figures 5 and 6). In the basin, the southern part of Unit 2 displays lateral variations of thickness from east to west (Figures 7 and 9). Unit 2 reaches a thickness of almost 1.3s TWT (~1040m thick) in its eastern part (Figure 11). The internal reflection pattern changes gradually from plane-parallel reflectors, low-amplitudes and low-frequency at its base to flat-lying, high amplitudes and high-frequency at its top (Figure 4). Its seismic facies, thickness and deformation pattern changes laterally within individual seismic lines. For example, the thickness can be about 0.6s TWT (~480m thick) southward and 1.2s TWT northward (see Figure 10). The most recent upper parts of Unit 4 are characterized by flat-lying strata that overlie Unit 2 strata in the deep basin (Figure 9).

4.2. Structural Analysis

4.2.1. Windward Passage Sill structural features

WPS area is characterized in seismic reflection profiles by a topographic high deformed by faults and series of folds (Figure 7). Numerous imbricated thrusts, mainly synthetic to the deformation front to the north (Figure 6, km 40 - 60), affect the acoustic basement and progressively steepen its northern slope. On the southern slope of the WPS, north dipping blind thrust faults are inferred from the geometry of the folded and shifted acoustic basement. Presently, gravity-driven normal faults shift the seafloor on the southern edge of the WPS as proposed by Rodriguez-Zurrunero et al. (2020).

A near-straight fault trace runs towards west along the north flank of the WPS (Figures 6, km 35-40, and Figure 7, km 70- 80). The recent study carried out by Rodríguez-Zurrunero et al. (2020) revealed that this fault strand seems to be aligned with the neotectonic SOFZ segment in the south flank of Septentrional Cordillera (Figure 1a). Its westward termination coincides with a narrow deformation zone with sub-vertical faults that displace the acoustic basement and the sediment layers in the central part of the WPS (wrench faults in Figure 12a, km 60-65). The deformation can be followed eastward on parallel seismic lines (Figures 7, km 70-77, and Figure12b, km 48-53) and interpreted as a positive flower structure oriented NW-SE. The overlying, parallel-bedded sediments appear to be tilted and displaced by the uplift of this positive flower structure (Figures 7 and 12a). This uplift of the seabed by the wrench fault strands of the flower structure created a wide synform located south of the wrench faults (Figures 2 and 12a). This synform is clearly observable in the seabed as an elongated east-west trending depression (Figure 2). In the westernmost part of the WPS, this positive flower structure takes the form of an NNW-SSE trending antiform with relief of about 350m (Figure 2). The

disturbance of the seafloor and shallow sediments indicate tectonic activity is currently occurring along this structure (Figure 12).

Confined between the WPS synform and the WPD, an isolated structural high characterizes the southwestern part of the WPS, named the WPS high (Figures 2, 5 and 7). This structural high is bound by opposing north- and south-dipping reverse faults (Figure 12a, km 35-50). These bounding reverse faults trending E-W with opposing ~45° dips delimit the WPS E-W high. The highly benched slope of the WPS, may be the direct consequence of activity on these reverse faults. However, the stepped morphology of the slope suggests that gravity-driven mechanisms may play an important role in its shape by promoting slope erosion (Figure 6, km 20-25).

4.2.2 The Windward Passage Deep structural features

SOFZ activity has clearly left a morphologic imprint on the seafloor study area (Figure 2) and affected the entire sedimentary record of the WPD area (Figures 5 to 11).

A network of reverse faults forms a small bulge and trough (1.5 km wide) (Figure 5, km 18-23). These faults are sub-vertical and seem to merge at depth along a main fault strand that may be associated with the SOFZ (Figure 9). The internal structure, which displays faults with an opposing dips on either side of this bulge, is typical of a positive flower structure (Figure 10, km 25-30). The main fault segments and several subordinate strands of this flower structure are imaged on the seafloor mainly as the edges of antiforms (Figure 2).

Expression of the SOFZ on seafloor of the WPD allows us to identify five distinct segments according to azimuth changes. The western 83-km-long segment, Segment 1 (S1 in Figure 1), runs offshore Cuba through the Punta Caleta high, from 74°50’W to 74°05’W and trends N82°E. A second 50-km-long segment (S2) runs from 74°10’W to 73°35’W and trends N83°E. Segments S1 and S2 have been considered as individual segments based on two distinct traces on the seismic sections and bathymetric data (Figures 1 and 2), despite short interruptions of rupture traces on the seabed (Figure 2). The boundary between S1 and S2 corresponds to a contractional jog which forms a relatively small bulge (about ~300m high, Figures 2 and 7), associated with a distinct change in azimuth of almost 1°. The boundary between Segments 2 and 3 is marked by a change of slope oriented N015° and a sharp azimuth change of 7-8° (Figure 2). Segment 3 is 74-km-long and trends N90°E. At its western end it runs along the rupture at 73°40’W. Eastward, over a distance of a few kilometers, the fault trace is characterized by a large azimuth change of 10°, that marks the boundary between S3 and S4. From 72°57’W, a Segment 4 trends N100°E to the south of the Tortue Island (Figure 1).

These active segments of the present-day SOFZ identified on the bathymetric map also appear at depth, in the seismic reflection data (identified on the figures by segments S1 to S4). The width of deformation associated with the SOFZ is narrower in the central part of the WPD (Figure 2, 73°40’W and 20°02’N) and wider at its extremities (6 km wide). Deformation linked to the flower structure spreads out eastward and the sedimentary cover is highly affected by its fault branches (Figures 6, 9, and 11). In this area, the most recent sedimentary units (Units 2 and 4) and the unconformities Uc4 and Uc4a appear to have been folded and faulted (Figures 6 and 11). The present-day offset and roughness of the seafloor indicate ongoing faulting in this area.

These E-W oriented SOFZ segments divides the WPD into a northern block, which we assume to be fixed, and an eastward-moving southern block. Deformation seems to be

concentrated in the northern block forming a perched sedimentary block (~10 to 20 km wide, Figures 7, km 30-45, and 5; km 20-40) characterized by a thick sedimentary deposit (about 1.2 s TWT, Figure 5). Upwarping of Units 1 and 2 and the folding along this perched sedimentary block, indicate that the WPD northern block is under a compressional stress field. The perched block is bound to the north by a southward-dipping normal fault that offsets the Units 1 and 2 and the acoustic basement (Figures 5, 6, 7 and 9). Unit 2 thickens northwards toward the fault, highlighting a syntectonic wedge related to an earlier stage of normal faulting (Figures 5 and 7).

At the southern boundary of the WPD, a set of reverse and thrust faults forms a ridge-like structural high (Figures 2 and 11, km 25-35). This feature is characterized in the bathymetric data by a steep, uniform, east-west trending scarp ridge. This ridge becomes higher eastward and seems to extend onshore. The scarp may correspond physiographically to the Môle de Saint-Nicolas area in the Northwestern Peninsula (Haiti) (Figures 1 and 2).

In summary, the seismic reflection profiles allowed us to establish a precise structural map of the Windward Passage Deep (Figures 2 and 13). The sedimentary and structural framework are much more complex than found in previous studies. Seismic data demonstrate that the WPD sedimentary cover is deformed by the multiple, near-vertical fault strands of the SOFZ, forming a large deformation corridor crossing the whole length of the basin (Figure 13).

5. Discussion

Our results reveal distinct deformation styles across the Windward Passage with several phases (at least 3 stages of deformation discussed in section 5.1). Thrust faults and folds in the deeper units of the WPS (Figure 6, km 25-45) are compatible with a predominantly contractional deformation phase, while the WPD thick sedimentary cover suggests an extensional deformation phase overprinted by a current transpressive deformation (e.g. Figure 6).

Strike-slip systems usually create conditions that allow for the juxtaposition of normal and reverse faults over a comparatively short distances and periods of time. The most likely hypothesis is a polyphase evolution with a compressive phase followed by a short extensional phase and then a recent transpressive phase. In this scenario, the normal faults offset the WPS southern border are the primary mechanism for WPD opening. Flower structures affecting the most recent WPD sedimentary record represent the current transpressive deformational style in the area.

5.1 Deformation events in the Windward Passage

Since the deformation patterns in the WPS and the WPD are quite different, we discuss them separately in this section, before proposing correlations and time constrains for both areas in section 5.2.

5.1.1 Windward Passage Sill

The folded Unit 1 records the first deformation event in the Windward Passage Sill domain (Figure 6). As proposed by Calais & Mercier de Lépinay (1995), folding of Units 1a, 1b and 1c (Figure 6) suggests that a contractional deformation pulse affected the WPS. The presence of minor unconformities within Unit 1 (unconformities Uc1a and Uc1b in Figures 6, 7 and 12) indicates intermittent episodes of erosion during its deposition. Units 1a, 2b and 3b are

broadly similar in style and orientation, which implies that their top unconformities correspond to rapid episodes of erosion.

The first episode of contractional deformation may have been active until the deposition of Unit 3, which displays less folding than the underlying unconformable Unit 1. The gentler folding of Unit 3 may be due to weaker contractional deformation, suggesting a second compressive pulse in the WPS.

Angular unconformity Uc4 separates the horizontally ponded strata of Unit 4 from the older folded layers of Units 1 and 3, highlighting a sedimentation hiatus (Figures 4 and 6). Overlying horizontal layers of Unit 4 suggest that the contractional deformation is less pronounced than the earliest contractional stages (Calais & Mercier de Lépinay, 1995). However, relatively flat reflectors do not mean a quiet period as proven by the presence of active reverse faults affecting Unit 4 in the WPS (Figure 5, km 40 - 60). The southward thickening of Unit 4 and tilting of unconformity Uc4 suggest ongoing contractional deformation (Figure 6). It implies a southward tilt of the WPS, possibly related to a recent activity of the imbricated thrust zone shearing off the WPS sedimentary strata on its northern slope (Figure 6, km 40-55). Such observations suggest an ongoing compressional stress field in WPS, in particular on its northern limit (Rodríguez-Zurrunero et al., 2020).

The positive flower structure in the middle part of the WPS provides evidence of a current strike-slip component in WPS area (Figures 12a, km 60-65, and Figure 12b, km 48-53)(Rodríguez-Zurrunero et al., 2020). Such a fault pattern, suggests that lateral slip, together with thrusting, are the two major styles of deformation operating in the WPS. Both styles of deformation reflect a transpressional tectonic regime that is likely a combined response of the large-scale present-day oblique collision between the Caribbean Plate and the Bahama Banks.

5.1.2 Windward Passage Deep

In contrast to the folding observed in the WPS, the Units 1 and 2 in the WPD seem relatively less disturbed by the early stages of compressional stress (Figure 6). At the northern edge of the WPD, the acoustic basement is tilted southward and the presence of northward dipping syntectonic wedges through the Unit 2 (Figures 6 and 7) suggests an early N-S extensional tectonics in the WPD area. This extensional stage probably follows Unit 1 deposition, which implies that the onset of Unit 1 deposition precedes the opening of the WPD area. A similar extensional stage affecting older folded sedimentary series is described by Calais & Mercier de Lépinay (1991) in the Imias Basin, just to the south of the study (Figure 1).

This early extensional tectonic event was related to the opening of the WPD domain and appears to have ceased after Unit 2 deposition. The normal fault identified at the northern boundary of the WPD seems presently inactive since the most recent overlying sediments in the WPD show no evidence of lateral thickening (Figures 5 and 6). The current morphology of WPD area seems to be controlled by transpressional regime with block “ramps” upward along both sides of the basin (Figure 9).

The neotectonic strike-slip regional component in the Windward Passage is apparent in the major SOFZ that crosses the entire length of the WPD (Figure 2). Sets of inward dipping faults that form part of this fault system converge at depth with the main SOFZ segments forming a large positive flower-structure (Figures 5 and 7). The positive flower structure formed

by transpressional shear reflects the current transpressional tectonic setting in the area. Because positive flower structures allow only a small amount of shortening, the dominant type of motion on a thoroughgoing fault characterized by this feature must be strike-slip with a transpressive component (Biddle & Christie-Blick, 1985). Our structural observations lead us to infer that the present-day WPD deformation pattern is currently ruled by significant transpression.

5.2 Tectonic interpretation of deformation events and onshore correlations

Due to the lack of direct sampling, sedimentary units in the Windward Passage can only be time-correlated based on onshore observations. Calais & Mercier de Lépinay (1995) were the first to time-correlate deformation events in the Windward Passage with four major paleogeographic periods in both southern Cuba and northern Hispaniola domains. The late Eocene, Oligocene, Middle Miocene and Late Pliocene paleogeographic stages are largely described onshore (Calais, 1990; Pindell & Draper, 1991; de Zoeten & Mann, 1991; Calais et al., 2016; Mann et al., 2002). Each one of these periods corresponds to a drastic reorganization of the Caribbean northern plate boundary geometry (Calais & Mercier de Lépinay, 1995). Based on recent kinematic and advances in onshore field work in southern Cuba (Rojas-Agramonte et al., 2008) and northern Hispaniola (Leroy et al., 2015; Escuder-Viruete et al., 2015; Escuder-Viruete & Pérez, 2020), we propose an alternative correlation of deformation stages in the Windward Passage with the four aforementioned paleogeographic framework in the northern Caribbean Plate (Figure 14).

5.2.1 Eocene Deformation: Piggyback basins phase

The acoustic basement high observed at the southern boundary of the WPD (Figure 11, km 25-35) may outcrop in the northwestern peninsula of Hispaniola . If this is the case, the acoustic basement sedimentary series would be the equivalent to the detrital sedimentary rocks of Abuillot Formation of Early/Middle Eocene (possibly Paleocene) age (Butterlin, 1960).

The Eocene is a period of intense contractional deformation with a broad overthrusting and progressive superposition of geologic formations in Cuba and Hispaniola (Mann et al., 1991; Iturralde-Vinent, 1994; Iturralde-Vinent & Gahagan, 2002; Rojas-Agramonte et al., 2008). The Cuban-Hispaniolan arc-continent collision with the Bahama Banks takes place in the Paleocene/middle Eocene (de Zoeten & Mann, 1991; Draper et al., 1994). During this time, the exhumation of ophiolitic and metamorphic rocks occurred, as well as the cessation of arc volcanism in Hispaniola (Escuder-Viruete et al., 2015). Structures in upper Paleocene to middle Eocene sedimentary rocks are consistent with an evolution from a forearc basin into piggy-back basins at the top of an advancing accretionary wedge (Escuder-Viruete et al., 2015). The folding and thrust faulting of Eocene rocks that induced regional uplift and associated piggy-back basins resulted from the convergence between the north-facing Hispaniola Island arc and the Bahama Banks (de Zoeten & Mann, 1991; Escuder-Viruete et al., 2015). The deformation style of the acoustic basement which is characterized by steep horizons, may reflect a complicated set of older stacked geological units inherited from this middle Eocene paleogeographic framework (Figure 3a). Enhanced uplift during the arc-continent collision may have resulted in subaerial exposure and formation of the basal angular unconformity Uc1 that cuts through previously tilted strata (Figure 6).

In the late Eocene, the WPS was probably the northernmost continuation of the early piggyback basin formed at the top of the accretionary wedge (Figure 14a, Pindell & Draper,

1991; Escuder-Viruete et al., 2015). Its current structure would thus be inherited from this compressive scenario. However, according to Escuder-Viruete et al. (2015), the progressive movement of the orogenic wedge toward the NE onto the continental margin may have produced a short subsidence period. This brief subsidence episode that took place in the Late Eocene must have created the space that accommodated deposition of Unit 1 above Uc1 (Figure 2a). Unconformities Uc1a and Uc1b were probably formed by local episodes of erosion, as the sub-units of Unit 1 are similar in both style and orientation (Figure 6). Outcrops of formations onshore suggest that this subsidence period was followed by deposition of deep-marine sequences (Upper Eocene to lower Miocene) in a relatively stable forearc basin.

5.2.2 Late-Oligocene: Extensional Phase

We interpret the extensional phase, that peaked during the earliest stages of development of the WPD, to be late Oligocene in age (Figures 3c and 14b). Disruption of Hispaniola and Eastern Cuban blocks started in Early Oligocene (Leroy et al., 2000). The eastern Cuban block becomes attached to the North American plate as the plate boundary jumps to the Oriente fault (Figure 3c, Leroy et al., 2000; Rojas-Agramonte et al., 2008; Wessels, 2019). Oligocene time is described as a tectonically stable period onshore without any significant compressional event on Hispaniola (Pindell & Draper, 1991; de Zoeten & Mann, 1991). However, several authors propose an extensional event related to the northern Caribbean boundary stress reorganization that occurred when the Oriente fault development during Oligocene (Calais & Mercier de Lépinay 1992; Iturralde-Vinent, 1998; Rojas-Agramonte et al., 2008). Onshore observations of Rojas-Agramonte et al. (2008) in the Sierra Maestra region suggest that contractional structures were overprinted by widespread extensional structures, mainly southward dipping normal faults, in the late Oligocene to Miocene (Figure 3c). Calais & Mercier de Lépinay (1991) also relate a transtentional regime in the offshore southern Cuban coast, which is accompanied significant subsidence of the Oriente deep. Normal faulting on the northern edge of the WPD is probably related to this transtensive episode (Figure 14b). Unit 1 and the acoustic basement are tilted toward the normal fault planes creating accommodation space for the syntectonic deposition of Unit 2 above the unconformity Uc2, which is likely late Eocene-Early Oligocene in age (Figures 3c et 14b). Syntectonic deposition of Unit 2 in the WPD may be coeval to the continuous Unit 1 deposition in the WPS area.

5.2.3 Middle Miocene Deformation: Compressional phase

We interpret the compressive episode in which Units 1 and 2 undergo contraction to be middle Miocene in age (Figures 3e and 14c). This event is mainly recorded in the WPS. According to Calais & Mercier de Lépinay (1991), a similar event is observed in the Oriente deep area (Figure 1a), where the basin sedimentary infill begins to undergo compression at this time. Extensional tectonic may have ceased in the early/middle Miocene times, when the onshore Oligocene basins sedimentary infill begins to fold (de Zoeten and Mann, 1999). From late Oligocene to early/middle Miocene time, the OFZ is the locus of large strike-slip faults, with only minor vertical movement (Figure 3d; de Zoeten and Mann, 1991). de Zoeten and Mann (1991) interpret the lack of angular unconformities during this interval as the lack of a significant contractional component. This interpretation is consistent with the oceanic spreading history in the Cayman Through, along the western extension of the Oriente Fault Zone (de Zoeten & Mann, 1991; Leroy et al., 2000). Oceanic magnetic anomalies in the Cayman Through suggest more

than 200km of left-lateral strike-slip displacement since late Oligocene-early Miocene time (Rosencrantz et al., 1988; Leroy et al., 2000).

Late Eocene-Early Miocene formations on Hispaniola (Altamira, Las Lavas, and La Toca Formations, e.g de Zoeten and Mann, 1991) are folded and faulted by a minor compressional episode during the middle Miocene (Pindell & Draper, 1991; de Zoeten & Mann, 1991; Calais & Mercier de Lépinay, 1995; Erikson et al., 1998; Escuder-Viruete & Pérez, 2020). This minor compressional event is associated with the initial development of a restraining bend in northern Hispaniola (Figure 3e) (Erikson et al., 1998; de Zoeten & Mann, 1991, 1999). As restraining bends do not efficiently accommodate the regional transcurrent shear of the fault system (Cooke et al., 2013), the middle Miocene was probably a period of active fault evolution including the abandonment and the development of new fault strands. Initiation of new fault strands in the WPS (Figure 3e) and its subsequent migration into the WPD (Figure 3f) may have allowed the fault system to more efficiency accommodate strike-slip stress. At this time, the whole of the Caribbean Plate to the south also experiences an episode of compression (Mauffret & Leroy, 1997; Mauffret & Leroy, 1999).

We propose that during this middle Miocene compressive episode, thrust faults formed in the WPS northern slope. Ongoing compression in the WPS, folded Unit 1 and created space to accommodate Unit 3 deposition (Figure 14c). Simultaneously, the SFZ strand evolved to accommodate part of the ongoing strike-slip stress (Figure 14c). Calais & Mercier de Lépinay (1995) propose an erosional episode during which Unit 1 may have been partially eroded and that the eroded material may have filled up the syncline depressions formed by the previous folding of Unit 1, thus depositing Unit 3. Another possible interpretation is that Unit 3 is the equivalent of the Upper Miocene to Lower Pliocene carbonate platform (Villa Trina Fm, e.g. Escuder-Viruete and Pérez, 2020) deposited during a transgressive cycle in the Lower Miocene to late-middle Pliocene in northern Hispaniola (Escuder-Viruete & Pérez, 2020). In the Cordillera Septentrional (Figure 1), the carbonate platform rocks are tilted, faulted and folded in synclines of the upper Eocene-middle Miocene age (Escuder-Viruete & Pérez, 2020). In this case, the local angular unconformity separating upper Eocene-middle Miocene rocks from less folded carbonate rocks onshore in the Cordillera Septentrional (de Zoeten and Mann, 1999) could be the equivalent of unconformity Uc3 observed in the WPS.

5.2.4 Pliocene to Present Deformation: Transpressional phase

We interpret the current transpressive component in the Windward Passage to have been initiated during Pliocene time (Figures 3f, 3g and 14d). The Pliocene is described as a period of dramatic reorganization of the northern Caribbean Plate boundary (Calais & Mercier de Lépinay, 1995; Calais et al., 2016). It is marked by the oblique collision of the northern Hispaniola block within the Bahama Banks (Figure 3f; Calais et al., 2016; Escuder-Viruete and Pérez, 2020). Obliquity of the maximum horizontal stress has promoted the development of a transpressional zone, with oblique motion between Hispaniola and Bahama Banks (Pindell & Draper, 1991). This, in turn, caused activation of WNW- to W-trending left-lateral strike-slip faults that accommodated and continue to accommodate part of the oblique convergence between the Caribbean and North American Plates. This may also be the case for the Septentrional Fault Zone (SFZ) which formed during the Pliocene as well (Figure 3g; Leroy et al., 2015; Calais et al., 2016; Escuder-Viruete and Pérez, 2020). Formation of the Septentrional-Orient Fault Zone (SOFZ) in the Windward Passage occured when the Oriente Fault Zone (OFZ) joined the

Septentrional Fault Zone (SFZ) (Figure 3f). The SOFZ segments in the WPD likely formed in the early Pliocene (Figure 14d). Transpressive deformation due to oblique collision prompted the development of positive flower structures in the Windward Passage (Figures 5, 6 and 7). In the WPD area, the positive flower structure forms an antiformal corridor over the SOFZ trace. Units 2 and 3 were folded and uplifted (Figure 14d) and this uplift created a strong erosional surface over the whole area, unconformity Uc4 (Figures 7 and 14d).

The Pliocene is also marked by the uplift of the Cordillera Septentrional (C. Sept. in Figure 3g, Calais et al., 2016; Escuder-Viruete and Pérez, 2020). The great regional uplift triggered the destruction of the upper Miocene-lower Pliocene forearc carbonate platform (Escuder-Viruete & Pérez, 2020). The onset of collision with the Bahama Banks during the mid-Pliocene in this area was followed by a regional sedimentary hiatus that persists until late Pleistocene in the northern Cordillera Septentrional (Escuder-Viruete and Pérez, 2020). We correlate the sedimentary hiatus highlighted by the overlying horizontal layers of Unit 4 above the folded Units 1 and 3 (unconformity Uc4 in Figures 4 and 6) to be the offshore equivalent of this regional sedimentary hiatus. If this is the case, Unit 4 would be middle- to late-Pleistocene in age. If so, the onshore equivalent would be the Quaternary coral reef terraces of northern Hispaniola (Isabela Fm, e.g. Escuder-Viruete and Pérez, 2020). This Quaternary formation that includes two main facies onshore, may correspond to Units 2a and 2b in the Windward Passage (Figures 4 and 8).

The system of Quaternary coral reef terraces on along the northwest coast of Hispaniola and the southeast coast of Cuban (Môle de St. Nicolas in Figure 1b; Sorel et al., 1991; Calais & Mercier de Lépinay, 1992) implies a period of active compressional tectonic uplift (Escuder-Viruete et al., 2020). The onshore extensions of the Western WPS high and of the Eastern WPD correspond to the uplifted areas of Guantánamo and Môle de St. Nicolas respectively (Figure 1b). The WPS displays enhanced uplift at its both extremities. Sorel et al. (1991) dates the most recent marine terrace at Môle de St. Nicolas as 80 Ka. In Cuba, Rojas-Agramonte et al. (2008) relate a general uplift of the reefs and detrital limestones from late Miocene to Quaternary as part of a system of marine terraces. The first Pleistocene terrace can be seen at several localities along the Cuban coast, with up to 20 m in Guantanamo area (southeastern Cuba coast, Figures 1 and 3). Marine terraces in Guantanamo are more elevated (up to 400 m, Muhs et al., 2017) than others described along Cuban coast supporting the notion of strong and rapid uplift (Iturralde-Vinent, 2003). Rojas-Agramonte et al. (2008) interpret this terrace to be related to active tectonic movements along the SOFZ.

Active reverse faults cutting the topmost layers of Unit 4 in the WPS high may be associated with the current compressional pulse recorded in the Northern Hispaniola. The collision with the Bahama Banks is also recorded by the formation of fold-thrust structures in the northwestern submarine accretionary wedge, known as the Northern Hispaniola Deformation Belt (NHDB in Figure 1a)(Dillon et al., 1992; Dillon et al., 1996; Rodríguez-Zurrunero et al., 2019). Southward tilting of Unit 4 could also be explained by this recent tectonic pulse in the Caribbean-North American Plate boundary that activated thrust faults along the northern limit of the WPS (Figure5, km 40-60). Moreover, the narrow positive flower structure affecting the most recent sedimentary layers in its middle part of the WPS indicates that the area is undergoing current transpressional deformation (Figure 2).

The presence of current transpressive structures across the Windward Passage area confirms the influence of the active transpressional strike-slip component in the area. An

oblique-reverse focal mechanism located in the WPD is evidence of transpression in this area (Corbeau et al., 2019). However, the regional approach of Corbeau et al. (2019) shows the scarcity of this type of event in the northern Caribbean Plate in which most focal mechanisms are thrust-fault related. The lack of focal mechanisms with left lateral strike-slip component may suggest that the accommodation of the horizontal component of displacement may be mostly aseismic (Rodríguez-Zurrunero et al., 2020) or that there are not enough seismometers to properly record it. Current compressional deformation is mainly N-S to NNE-SSW as the result of the collision between the Bahama Banks and Hispaniola (Corbeau et al., 2019).

5.2.2 Timing constraints for the SOFZ propagation

The closely spaced seismic lines crossing the SOFZ main segments allowed us to infer critical time indicators that bracket the interval in the stratigraphic section during which horizontal strike-slip motion began in the WPD. As the Early Miocene locus of Caribbean North-American Plate displacement was north of the Cordillera Septentrional (Figure 3d)(Calais & Mercier de Lépinay, 1995; Erikson et al. 1998), the strike-slip displacement may not have affected the early WPD sedimentary record at this time.

Geometry trends of Units 1 and 2 suggest that these two units predate initiation of horizontal movement on the SOFZ in the WDP (Figures 5 and 10). Strike-slip motion of S1, S2, S3 and S4 segments appears to have taken place after Units 1 and 2 were deposited (Figure 1b). The approximately E-W trending of these segments divides the WPD into a southern block and a northern block moving past each other as left-lateral strike-slip movement occurs on the fault system. Thickness changes in Unit 2 between the WPD northern and southern blocks may be due to the left-lateral southern block displacement (Figures 5, 10, and 11). Bohannon (1975) describes a similar observation elaborated by the correlation of Oligocene and Miocene rocks in southern California. In this region, these formations were originally deposited in continuous nonmarine basin formed by extentional tectonics, but subsequent right-slip faults evolved and have displaced these formations to their present positions. More examples are described in the Wecoma fault in the Cascadia basin, in the offshore Oregon convergent margin (Goldfinger et al., 1996), and at strike-slip fault zones in the offshore regions of Fukushima and Miyagi, Japan (Arato, 2017).

Unit 2 thickness and seismic facies are used to estimate the left-lateral strike-slip displacement since the inception of the SOFZ segments. Basin configuration before strike-slip fault propagation should be identifiable after restoration of left slip displacement (Goldfinger et al., 1996). The horizontal plane sections are restored to estimate the onset of strike-slip motion. The southern block is translated right-laterally until Unit 2 thickness and seismic facies match on the opposite side of the fault. Corresponding Unit 2 thickness and seismic facies are found on seismic lines separated by 80 km in Figures 11 and 5, thus the horizontal distance needed to restore the section is at least ~80 km (Figure 15). However, as each fault strand accommodates part of the lateral relative motion, the left-lateral displacement of this unit must have taken place over a much larger deformation zone rather than along a single fault segment (Figure 15). We infer an age of 5.4 ± 0.2 Ma for the onset of SOFZ segments in the WPD. Our estimate is based on the current ~14–15 mm $yr^{-1}$of left-lateral motion predicted by Benford et al. (2012) for the Oriente Fault and our estimation of 80 km-net slip in the WPD. Time of fault propagation in the WPD is then coincident with the Pliocene paleogeographic reorganization. This estimated fault age may include a large error as we consider a slip-rate constant since the late Miocene time.

Even though it is known that strike-slip fault systems change the apportionment of fault slip rates as they evolve and some slip rate discrepancy may occur over time (Cooke et al., 2020).

Timing relationship between Oriente and Septentrional fault segments (OFZ and SFZ respectively, e.g. Figure 3) is not clear. According to Calais & Mercier de Lépinay (1995) the plate boundary has been migrating since Late Oligocene-Early Miocene time when the locus of Caribbean-North American Plate motion shifted to the Oriente fault and splayed eastward (Figure 3f). The transcurrent plate boundary must have been located north of Hispaniola during the Miocene until the Pliocene (Calais & Mercier de Lépinay, 1995). However, Pliocene oblique collision of the Bahama Banks with northern Hispaniola (Escudier-Viruete and Perez, 2020) slowed down the Hispaniola's eastward motion with respect to the North American Plate (Calais et al., 1992). Obliquity of the collision transmitted far-field stress to the overriding plate and prompted activation of strike-slip and contractional components within Hispaniola. Partitioning of the external stress field caused activation of the SFZ and uplift of the Cordillera Septentrional (Figures 3g and 3f, Mann et al., 2002; Calais et al., 2016). Because of SFZ formation, the previously location of the major strike-slip fault in the Hispaniola basin was abandoned (Calais & Mercier de Lépinay, 1995). The major strike-slip motion shifted south to the present-day trace of the plate boundary, transferring part of northern Hispaniola (the present-day Cordillera Septentrional of the Dominican Republic) to the North-American plate (Calais & Mercier de Lépinay, 1995; Erikson et al., 1998; Leroy et al., 2015; Calais et al., 2016; Escudier-Viruete & Perez, 2020).

Our estimate of the age of the SOFZ segments in the WPD correlates well with ages inferred for onshore strike-slip faults on Hispaniola (Draper et al., 1994; Erikson et al., 1998, Escudier-Viruete and Perez, 2020). Erikson et al. (1998) estimate a similar offset of 85 km for the Septentrional fault segment in Cibao basin in the Cibao Valley (northern Hispaniola, Figure 1). Escudier-Viruete and Perez (2020) suggests a similar horizontal displacement of ~88 km, which implies an average ~25 mm. yr^{-1}slip rate for the last 3.5 Ma. Draper et al. (1994) related that the CFZ (subparallel to the onshore SFZ; Figure 3g) has accommodated at least 60 km of left-lateral strike-slip since the Eocene. During the Pliocene collision, the major strike-slip motion probably shifted south to the SFZ present location (Calais et al., 2016) as the Oriente fault system splayed eastward running across the WPD and into northern Hispaniola to form the SOFZ (Figure 3f; Calais & Mercier de Lépinay, 1995; Leroy et al., 2015). Moreover, the estimate 16.5 km offset along the Septentrional fault zone segment offshore does presume an onset of motion at 1.8 Ma (Leroy et al., 2015).

These discrepancies of displacements imply that until the uppermost Pliocene, the regional stress field is accommodated mainly by the SFZ but that some local-field stress transferred to subparallel splays, such as the Camú fault zone (Figure 1a)(Rodríguez-Zurrunero et al., 2020). However, in the uppermost Pliocene the trace of the OFZ extends offshore parallel to the northern coast of Haiti until it connects with the SFZ in northwestern Dominican Republic (Figure 3f, Leroy et al., 2015). The result of this last regional paleogeographic reorganization formed the current plate boundary which is represented by the SOFZ present-day trace (Figure 3g; Calais et al., 1992; Leroy et al., 2015; Calais et al., 2016). The uppermost Pliocene is also the age inferred by Escudier-Viruete and Perez (2020) for the oblique collision of the Bahama Banks with the northern Hispaniola.

5 Conclusions

Tectono-sedimentary evolution in the Windward Passage provides critical constraints for the diachronous evolution of the northern Caribbean Plate boundary over Neogene times. Four main seismic units were identified above the acoustic basement in the Windward Passage. Sedimentation in the Windward Passage Sill (WPS) and in the Windward Passage Deep (WPD) probably occurred in a common palegeographic framework until the inception of the early Oriente Fault zone (OFZ). Therefore, syntectonic deposition of Unit 2, distinct to the WPD, marks the beginning of strike-slip stress field in the area. Discrepancies in seismic facies and the deformation patterns present in the seismic units in both geographic areas probably reflects the structural evolution of the earlier transcurrent plate boundary represented by the OFZ until the initiation of the current SOFZ.

The Windward Passage has recorded at least 4 tectonic events related to the ongoing oblique collision between the Caribbean Plate and the Bahama Banks. In this context, the first tectonic event in the area may correspond to the period of Cuban-Hispaniola Arc collision, in which the sedimentary cover of the ancient forearc basin was gradually uplifted recording the formation of piggyback basins along a syn-collisional margin. The second tectonic event records a period of transition between mainly contractional and transcurrent motions. This period is marked by an important paleogeographic reorganization that corresponds to a brief transtentional event that resulted in the opening of the Windward Passage Deep during the OFZ initiation and the consequent disruption of the Cuban and Hispaniola blocks. The last two events are characterized by contractional and then the current transpressional deformation mainly reflects (i) the progressive collision between the Bahama Banks and Hispaniola blocks and (ii) the Caribbean Plate's eastward escape relative to the North American plate. These last stages of deformation are particularly well recorded in the Windward Passage sedimentary cover, which was folded and displaced left-laterally shifted by the SOFZ. Through the Windward Passage Deep, the estimated ~80 km offset of the sedimentary cover on either side of the major fault suggests an early Pliocene inception for the SOFZ segments in this area. This result provides important time constraints on the SOFZ southeastward migration as well as additional information on the time-related evolution of the northern Caribbean Plate boundary.

Acknowledgments

We thank Captain Moimeaux, the crews and technicians of the RV L'Atalante (IFREMER/GENAVIR) and the scientific team. We are indebted to the French Embassies in Haiti, Bruno Asseray and Cuba, Aurelie Nogues and Oliver Tenes. We also thank the local authorities, as well as Daysarih Tapanes Robau from CITMA, Claude Prepetit from BME, and R. Momplaisir, D. Boisson and J. Jadotte from UEH. We thank Dr Bernard Mercier de Lépinay for his precious time and helpful comments. We also want to thank the Associate Editor Dr Laura Giambiagi, and the reviewers Dr Jose-Luis Granja Bruña and Dr Serge Lallemand for their helpful comments on the first version of this paper. We deeply thank Dr Heather Sloan for post-editing the English style and grammar. A. Oliveira de Sá is supported by funding from Sorbonne University. The processed data will be available on demand on the website Seanoe.org.

References

Arato, H. (2017). Cenozoic Fault Zone Activity and Geologic Evolution of the Offshore Regions of Fukushima and Miyagi Prefectures, Northeastern Japan, Based on Petroleum

687 Exploration Data. In Y. Itoh (Ed.), *Evolutionary Models of Convergent Margins - Origin*
688 *of Their Diversity* (pp. 29-48). Croatia: IntechOpen. http://dx.doi.org/10.5772/67391
689 Benford, B., DeMets, C., & Calais, É. (2012). GPS estimates of microplate motions, northern
690 Caribbean: evidence for a Hispaniola microplate and implications for earthquake hazard.
691 *Geophysical Journal International*, 191(2), 481–490. https://doi.org/10.1111/j.1365-
692 246X.2012.05662.x
693 Biddle, K. T., & Christie-Blick, N. (Eds.) (1985). *Strike-Slip Deformation, Basin Formation, and*
694 *Sedimentation*. Tulsa, OK: SEPM Society for Sedimentary Geology.
695 https://doi.org/10.2110/pec.85.37
696 Bohannon, R.G. (1975). Mid-Tertiary conglomerates and their bearing on Transverse Range
697 tectonics, southern California, in J.C. Crowell (Ed.), *San Andreas fault in southern*
698 *California - a guide to San Andreas fault from Mexico to Carrizo Plain* (Special Report
699 118, p. 75-82): Sacramento, CA: Division of Mines and Geology.
700 Boschman, L. M., van Hinsbergen, D. J. J., Torsvik, T. H., Spakman, W., & Pindell, J. L. (2014).
701 Kinematic reconstruction of the Caribbean region since the Early Jurassic. *Earth-Science*
702 *Reviews*, 138, 102–136. https://doi.org/10.1016/j.earscirev.2014.08.007
703 Butterlin, J. (1960). Géologie régionale de la République D'Haïti. In J. Butterlin (Ed.), Géologie
704 générale et régionale de la république d'Haïti (pp. 29-118). Paris: Éditions de l'IHEAL.
705 Calais, É. (1990). Relations cinématique/déformation le long des limites de plaques en
706 coulissage : l'exemple de la limite de plaques Nord Caraïbe de Cuba à Porto Rico,
707 (Doctoral dissertation). Nice: University of Nice.
708 Calais, É., Béthoux, N., de Lépinay, B.M. (1992). From transcurrent faulting to frontal
709 subduction: a seismotectonic study of the Northern Caribbean Plate Boundary from Cuba
710 to Puerto Rico. Tectonics. 11(1), 114-123. https://doi.org/10.1029/91TC02364."
711 Calais, É., & Mercier de Lépinay, B. (1989). Des données nouvelles sur la Cordillère
712 Septentrionale de République Dominicaine: ses relations avec la limite de plaques
713 décrochante. *Comptes rendus de l'Académie des sciences*, 309, 409–415.
714 Calais, É., & Mercier de Lépinay, B. (1991). From transtension to transpression along the
715 northern Caribbean plate boundary off Cuba: implications for the Recent motion of the
716 Caribbean plate. *Tectonophysics*, 186(3), 329–350. https://doi.org/10.1016/0040-
717 1951(91)90367-2
718 Calais, É., & Mercier de Lépinay, B. (1992). La limite de plaques décrochante Nord Caraïbe en
719 Hispaniola: évolution paléogéographique et structurale cénozoïque. *Bull. Soc. Géol*,
720 3(163), 309–324.
721 Calais, É., & Mercier de Lépinay, B. (1995). Strike-slip tectonic processes in the northern
722 Caribbean between Cuba and Hispaniola (Windward Passage). *Marine Geophysical*
723 *Researches*, 17(1), 63–95. https://doi.org/10.1007/BF01268051
724 Calais, É., Freed, A., Mattioli, G., Amelung, F., Jónsson, S., Jansma, P., et al. (2010).
725 Transpressional rupture of an unmapped fault during the 2010 Haiti earthquake. *Nature*
726 *Geoscience*, 3(11), 794–799. https://doi.org/10.1038/ngeo992
727 Calais, É., Symithe, S., Mercier de Lépinay, B., & Prépetit, C. (2016). Plate boundary
728 segmentation in the northeastern Caribbean from geodetic measurements and Neogene
729 geological observations. *Comptes Rendus Geoscience*, 348(1), 42–51.
730 https://doi.org/10.1016/j.crte.2015.10.007
731 Chemenda, A. I., Burg, J.-P., & Mattauer, M. (2000). Evolutionary model of the Himalaya–Tibet
732 system: geopoem: based on new modelling, geological and geophysical data. *Earth and*

Planetary Science Letters, 174(3), 397–409. https://doi.org/10.1016/S0012-821X(99)00277-0

Cooke, M. L., Schottenfeld, M. T., & Buchanan, S. W. (2013). Evolution of fault efficiency at restraining bends within wet kaolin analog experiments. *Journal of Structural Geology*, 51, 180–192. https://doi.org/10.1016/j.jsg.2013.01.010

Cooke, M. L., Toeneboehn, K., & Hatch, J. L. (2020). Onset of slip partitioning under oblique convergence within scaled physical experiments. *Geosphere*, 16(3), 875–889. https://doi.org/10.1130/GES02179.1

Corbeau, J., Rolandone, F., Leroy, S., Meyer, B., Mercier de Lépinay, B., Ellouz-Zimmermann, N., et al. (2016). How transpressive is the northern Caribbean plate boundary?. *Tectonics*, 35(4), 1032-1046. https://doi.org/10.1002/2015TC003996

Corbeau, J., Gonzalez, O., Clouard, V., Rolandone, F., Leroy, S., Keir, D., et al. (2019). Is the local seismicity in western Hispaniola (Haiti) capable of imaging northern Caribbean subduction? *Geosphere*, 15 (6), 1738–1750. https://doi.org/10.1130/GES02083.1

DeMets, C. (1992). Oblique convergence and deformation along the Kuril and Japan Trenches, J. Geophys. Res., 97(B12), 17615– 17625. https://doi.org/10.1029/92JB01306

de Zoeten, R., & Mann, P. (1991). Structural geology and Cenozoic tectonic history of the central Cordillera Septentrional, Dominican Republic. In Geological Society of America Special Papers (Vol. 262, pp. 265–280). *Geological Society of America*. https://doi.org/10.1130/SPE262-p265

de Zoeten, R., & Mann, P. (1999). Chapter 11 Cenozoic el mamey group of northern hispaniola: a sedimentary record of subduction, collisional and strike-slip events within the north America-Caribbean plate boundary zone. In P. Mann (Ed.), Sedimentary Basins of the World (Vol. 4, pp. 247–286). Elsevier. https://doi.org/10.1016/S1874-5997(99)80045-8

Dillon, W. P., Austin, J. A., Scanlon, K. M., Terence Edgar, N., & Parson, L. M. (1992). Accretionary margin of north-western Hispaniola: morphology, structure and development of part of the northern Caribbean plate boundary. *Marine and Petroleum Geology*, 9(1), 70–88. https://doi.org/10.1016/0264-8172(92)90005-Y

Dillon, W., Edgar, N., Scanlon, K., & Coleman, D. (1996). A Review of the Tectonic Problems of the Strike-Slip Northern Boundary of the Caribbean Plate and Examination by GLORIA. In J. Gardner, M. Field, & D. Twichell (Eds.), *Geology of the United States' Seafloor: The View from GLORIA* (pp. 135-164). Cambridge: Cambridge University Press. https://doi.org/10.1017/CBO9780511529481.013

Draper, G., Mann, P., & Lewis, J. F. (1994). Hispaniola. In S. K. Donovan & T. A. Jackson (Ed.), *Caribbean Geology: An Introduction* (pp. 129–150). Jamaica, CA: University of the West Indies Publishers Association.

Erikson, J., Pindell, J., Karner, G., Sonder, L., Fuller, E., & Dent, L. (1998). Neogene Sedimentation and Tectonics in the Cibao Basin and Northern Hispaniola: An Example of Basin Evolution Near A Strike-Slip-Dominated Plate Boundary. *The Journal of Geology*, 106(4), 473-494. https://doi.org/10.1086/516036

Escuder-Viruete, J., Suárez-Rodríguez, A., Gabites, J., & Pérez-Estaún, A. (2015). The Imbert Formation of northern Hispaniola: a tectono-sedimentary record of arc-continent collision and ophiolite emplacement in the northern Caribbean subduction-accretionary prism. *Solid Earth Discussions*, 7(2), 1827–1876. https://doi.org/10.5194/sed-7-1827-2015

Escuder-Viruete, J., & Pérez, Y. (2020). Neotectonic structures and stress fields associated with oblique collision and forearc sliver formation in northern Hispaniola: Implications for the

seismic hazard assessment. *Tectonophysics*, 784, 228-452. https://doi.org/10.1016/j.tecto.2020.228452

Escuder-Viruete, J., Beranoaguirre, A., Valverde-Vaquero, P., McDermott, F.(2020). Quaternary deformation and uplift of coral reef terraces produced by oblique subduction and underthrusting of the Bahama Platform below the northern Hispaniola forearc. Tectonophysics, 796. https://doi.org/10.1016/j.tecto.2020.228631.

Fitch, T. J. (1972). Plate convergence, transcurrent faults, and internal deformation adjacent to Southeast Asia and the western Pacific. *Journal of Geophysical Research*, 77(23), 4432–4460. https://doi.org/10.1029/JB077i023p04432

Goldfinger, C., Kulm, L. D., Yeats, R. S., Appelgate, B., MacKay, M., & Cochrane, G. R. (1996). Active strike-slip faulting and folding of the Cascadia plate boundary and forearc in central and northern Oregon. In A.M. Rogers, T. J. Walsh, W. J. Kockelman, and G. Priest (Eds.), Assessing and Reducing Earthquake Hazards in the Pacific Northwest, U.S. Geol. Surv. Prof. Pap. (Vol. 2, pp. 223-256). Denver, CO: U.S. Geological Survey. https://doi.org/10.3133/pp1560

Gordon, M. B., Mann, P., Cáceres, D., & Flores, R. (1997). Cenozoic tectonic history of the North America-Caribbean plate boundary zone in western Cuba. *Journal of Geophysical Research: Solid Earth*, 102(B5), 10055–10082. https://doi.org/10.1029/96JB03177

Goreau, P. D. (1989). The tectonic evolution of the North Central Caribbean plate margin.

Granja Bruña, J. L., Carbó-Gorosabel, A., Llanes Estrada, P., Muñoz-Martín, A., ten Brink, U. S., Gómez Ballesteros, M., et al. (2014). Morphostructure at the junction between the Beata ridge and the Greater Antilles island arc (offshore Hispaniola southern slope). *Tectonophysics*, 618, 138–163. https://doi.org/10.1016/j.tecto.2014.02.001

Iturralde-Vinent, M. A. (1994). Cuban Geology: A New Plate-Tectonic Synthesis. *Journal of Petroleum Geology*, 17(1), 39–69. https://doi.org/10.1111/j.1747-5457.1994.tb00113.x

Iturralde-Vinent, M.A. (1998). Sinopsis de la constitución geológica de Cuba. *Acta Geologica Hispanic*a, 33, 9–56.

Iturralde-Vinent, M., & Macphee, R. (1999). Paleogeography of the Caribbean Region: Implications for Cenozoic biogeography. *Bulletin of the American Museum of Natural History*, 238, 1–95.

Iturralde-Vinent, M. A. (2003). *Ensayo sobre la paleogeografía del Cuaternario de Cuba*. Paper presented at the V Congreso Cubano de Geología y Minería, Memorias Geomin, La Habana.

Iturralde-Vinent, M., & Gahagan, L. (2002). Latest Eocene to Middle Miocene tectonic evolution of the Caribbean: Some principles and their implications for plate tectonic modeling. In T. A. Jackson (Ed.), *Caribbean geology into the third millennium: Transactions of the Fifteenth Caribbean Geological Conference* (pp. 47–62), Kingston: University of the West Indies Press.

Jarrard, R. D. (1986). Terrane motion by strike-slip faulting of forearc slivers. *Geology*, 14(9), 780-783. https://doi.org/10.1130/0091-7613(1986)14<780:TMBSFO>2.0.CO;2

Lallemand, S., Liu, C.-S., Dominguez, S., Schnürle, P., Malavieille, J., and the ACT scientific crew. (1999). Trench-parallel stretching and folding of forearc basins and lateral migration of the accretionary wedge in the southern Ryukyus: A case of strain partition caused by oblique convergence; Tectonics, 18 (2), 231-247. doi:10.1029/1998TC900011

Laurencin, M., Marcaillou, B., Graindorge, D., Lebrun, J. -F., Klingelhoefer, F., Boucard, M., et al. (2019). The Bunce Fault and Strain Partitioning in the Northern Lesser Antilles.

Geophysical Research Letters, 46(16), 9573–9582. https://doi.org/10.1029/2019GL083490

Leroy, S., Mercier de Lépinay, B., Mauffret, A., & Pubellier, M. (1996). Structural and Tectonic Evolution of the Eastern Cayman Trough (Caribbean Sea) From Seismic Reflection Data. *AAPG Bulletin*, 80(2). 222-247. https://doi.org/10.1306/64ED8796-1724-11D7-8645000102C1865D

Leroy, S., Mauffret, A., Patriat, P., & Mercier de Lépinay, B. (2000). An alternative interpretation of the Cayman trough evolution from a reidentification of magnetic anomalies. *Geophysical Journal International*, 141(3), 539–557. https://doi.org/10.1046/j.1365-246x.2000.00059.x

Leroy, S. (2012). HAITI-SIS cruise,L'Atalante R/V. https://doi.org/10.17600/12010070

Leroy, S., & Ellouz-Zimmermann, N. (2013). HAITI-SIS2 cruise, L'Atalante R/V. https://doi.org/10.17600/13010080

Leroy, S., Ellouz-Zimmermann, N., Corbeau, J., Rolandone, F., Mercier de Lépinay, B., Meyer, B., et al. (2015). Segmentation and kinematics of the North America-Caribbean plate boundary offshore Hispaniola. *Terra Nova*, 27(6), 467–478. https://doi.org/10.1111/ter.12181

Mann, P., Taylor, F. W., Edwards, R. L., & Ku, T.-L. (1995). Actively evolving microplate formation by oblique collision and sideways motion along strike-slip faults: An example from the northeastern Caribbean plate margin. *Tectonophysics*, 246(1), 1–69. https://doi.org/10.1016/0040-1951(94)00268-E

Mann, P., Prentice, C., Burr, G., Peña, L., & Taylor, F. (1998). Tectonic geomorphology and paleoseismology of the Septentrional fault system, Dominican Republic. In J.F Dolan & P. Mann (Eds.), *Active Strike-Slip and Collisional Tectonics of the Northern Caribbean Plate Boundary Zone*, *Geological Society of America Special Papers* (Vol. 326, pp. 63-124). Boulder, Colo: GSA Books. https://doi.org/10.1130/0-8137-2326-4.63

Mann, P., Draper, G., & Lewis, J. F. (1991). An overview of the geologic and tectonic development of Hispaniola, *Geological Society of America Special Papers,* 262, 1–28. https://doi.org/10.1130/SPE262-p1

Mann, P., Calais, É., Ruegg, J.-C., DeMets, C., Jansma, P. E., & Mattioli, G. S. (2002). Oblique collision in the northeastern Caribbean from GPS measurements and geological observations. *Tectonics*, 21(6), 1057–1083. https://doi.org/10.1029/2001TC001304

Mauffret, A., & Leroy, S. (1997). Seismic stratigraphy and structure of the Caribbean igneous province. *Tectonophysics*, 283(1), 61–104. https://doi.org/10.1016/S0040-1951(97)00103-0

Mauffret, A., & Leroy, S. (1999). Neogene intraplate deformation of the caribbean plate at the beata ridge. In P. Mann (Ed.), *Sedimentary Basins of the World* (Vol. 4, pp. 627–669), *Elsevier*. https://doi.org/10.1016/S1874-5997(99)80055-0

Muhs, D. R., Schweig, E. S., Simmons, K. R., & Halley, R. B. (2017). Late Quaternary uplift along the North America-Caribbean plate boundary: Evidence from the sea level record of Guantanamo Bay, Cuba. *Quaternary Science Reviews*, 178, 54–76. https://doi.org/10.1016/j.quascirev.2017.10.024

Mullins, H. T., Breen, N., Dolan, J., Wellner, R. W., Petruccione, J. L., Gaylord, M., et al. (1992). Carbonate platforms along the southeast Bahamas-Hispaniola collision zone. *Marine Geology*, 105(1), 169–209. https://doi.org/10.1016/0025-3227(92)90188-N

Philippon, M., & Corti, G. (2016). Obliquity along plate boundaries. *Tectonophysics*, 693, 171–182. https://doi.org/10.1016/j.tecto.2016.05.033

Pindell, J., Kennan, L., Maresch, W. V., Stanek, K.-P., Draper, G., & Higgs, R. (2005). Plate-kinematics and crustal dynamics of circum-Caribbean arc-continent interactions: Tectonic controls on basin development in Proto-Caribbean margins. In H. G. A. Lallemant & V. B. Sisson (Ed.), *Caribbean-South American plate interactions*, Venezuela. CA: Geological Society of America. https://doi.org/10.1130/0-8137-2394-9.7

Pindell, J. L., & Draper, G. (1991). Stratigraphy and geological history of the Puerto Plata area, northern Dominican Republic. In P. Mann, G. Draper, J. F. Lewis (Eds.), *Geologic and Tectonic Development of the North America-Caribbean Plate Boundary in Hispaniola*, *Geological Society of America Special Papers* (Vol. 262, pp. 97–114). https://doi.org/10.1130/SPE262-p97

Rodríguez-Zurrunero, A., Granja-Bruña, J. L., Carbó-Gorosabel, A., Muñoz-Martín, A., Gorosabel-Araus, J. M., Gómez de la Peña, L., et al. (2019). Submarine morpho-structure and active processes along the North American-Caribbean plate boundary (Dominican Republic sector). *Marine Geology*, 407, 121–147. https://doi.org/10.1016/j.margeo.2018.10.010Rodríguez-Zurrunero, A., Granja-Bruña, J. L., Muñoz-Martín, A., Leroy, S., ten Brink, U., Gorosabel-Araus, J. M., et al. (2020). Along-strike segmentation in the northern Caribbean plate boundary zone (Hispaniola sector): Tectonic implications. *Tectonophysics*, 776, 228-322. https://doi.org/10.1016/j.tecto.2020.228322

Rojas-Agramonte, Y., Neubauer, F., Garcia-Delgado, D. E., Handler, R., Friedl, G., & Delgado-Damas, R. (2008). Tectonic evolution of the Sierra Maestra Mountains, SE Cuba, during Tertiary times: From arc-continent collision to transform motion. *Journal of South American Earth Sciences*, 26(2), 125–151. https://doi.org/10.1016/j.jsames.2008.05.005

Rosencrantz, E., Ross, M. I., & Sclater, J. G. (1988). Age and spreading history of the Cayman Trough as determined from depth, heat flow, and magnetic anomalies. *Journal of Geophysical Research: Solid Earth*, 93(B3), 2141–2157. https://doi.org/10.1029/JB093iB03p02141

Sorel, D., Purser, B. H., & Senatos, H. (1991). Strike-slip tectonic processes in the northern Caribbean between Cuba and Hispaniola (Windward Passage). Essai de Datation Des Récifs Soulevés d'Haiti Par La Méthode Du Forcage Climatique Orbital. *Comptes rendus de l'Académie des sciences*, 313, 1277–1281.

Syed Tabrez, A., Freed, A. M., Calais, É., Manaker, D. M., & McCann, W. R. (2008). Coulomb stress evolution in Northeastern Caribbean over the past 250 years due to coseismic, postseismic and interseismic deformation. *Geophysical Journal International*, 174(3), 904–918. https://doi.org/10.1111/j.1365-246X.2008.03634.x

Symithe, S., Calais, É., Chabalier, J. B., Robertson, R., & Higgins, M. (2015). Current block motions and strain accumulation on active faults in the Caribbean. *Journal of Geophysical Research: Solid Earth*, 120(5), 3748–3774. https://doi.org/10.1002/2014JB011779

ten Brink, U., & Lin, J. (2004). Stress interaction between subduction earthquakes and forearc strike-slip faults: Modeling and application to the northern Caribbean plate boundary. *Journal of Geophysical Research: Solid Earth*, 109, B12310. https://doi.org/10.1029/2004JB003031

Teyssier, C., Tikoff, B., & Markley, M. (1995). Oblique plate motion and continental tectonics. *Geology*, 23(5), 447–450. https://doi.org/10.1130/0091-7613(1995)023<0447:OPMACT>2.3.CO;2

Wessels, R. J. F. (2019). Chapter 15 - Strike-Slip Fault Systems Along the Northern Caribbean Plate Boundary. In J. C. Duarte (Ed.), *Transform Plate Boundaries and Fracture Zones* (pp. 375–395). Elsevier. https://doi.org/10.1016/B978-0-12-812064-4.00015-3

Figure Captions

Figure 1. Tectonic map of the northern Caribbean plate boundary. (a) Orange dots indicate the presumed epicenters of Mw > 7 historical earthquakes (from Syed Tabrez et al., 2008). Velocities in mm. a−1 are reported from a block model incorporating the available GPS data, velocity vectors are relative to the North American plate (Benford et al., 2012). The parts of the fault system studied in this paper are outlined in red. Red line with black dots represent the fault strand identified by Rodríguez- Zurrunero et al. (2020) in the Windward Passage Sill (WPS). Faults in black are from previous studies (Calais & Mercier de Lépinay, 1989, 1991; Corbeau et al., 2016; Leroy et al., 2015; Granja Bruña et al., 2014; Leroy et al., 1996; Mann et al., 1995, 1998; Mauffret & Leroy, 1997). Inset: Geodynamic map. NOAM: North American plate; CAR: Caribbean plate; MB: Muertos Belt; MCSC: Mid-Cayman spreading center; CT: Cayman trough; D.R.: Dominican Republic; OFZ: Oriente Fault zone; EPGFZ: Enriquillo–Plantain Garden Fault zone; WFZ: Walton Fault zone; SDB: Santiago Deformed Belt; BB: Bahamas platform; BR: Beata Ridge (modified from Leroy et al., 2015). (b) Bathymetric map of the Windward Passage area showing the active segments of the Oriente-Septentrional Fault Zone (SOFZ) inferred from distinct geometric fault complexities. Active SOFZ Segments are outlined in red. Blue lines represent the seismic sections collected during cruises HAITI-SIS 1-2(Leroy, 2012; Leroy & Ellouz-Zimmermann, 2013; Leroy et al., 2015). Bold pink and blue lines indicate positions of seismic sections in this paper (Figures 5 and 13). Boxe of detailed bathymetry (Figure 2). EPGFZ: Enriquillo-Plantain-Garden Fault Zone; NHDB: Northern Hispaniola Deformation Belt; SOFZ: Septentrional–Oriente fault zone, WPS: Windward Passage Sill, WPD: Windward Passage Deep

Figure 2. (a) Detailed bathymetric map of the Windward Passage Sill and Deep areas. (b) Bathymetric map with structural interpretations. See Figure 1 for location of the map. In the Windward Passage Sill area, the activity of wrench faults forms a relief about 350 m high structured by an antiform and a synform trending E-W and NW-SE . The Septentrional Oriente Fault Zone (SOFZ) represented in bold red lines by the S1 to S4 fault segments, cross-cuts the Windward Passage Deep area. Red arrows show the average plate convergence direction of the North American plate with respect to the Caribbean (Calais et al., 2016). Multibeam bathymetry data from the HAITI-SIS cruises and NORCARIBE (Leroy, 2012; Leroy and Ellouz-Zimmermann, 2013; Leroy et al., 2015; Granja-Bruna et al 2014) completed with the GEBCO Digital Atlas (https://www.gebco.net/data_and_products/gebco_digital_atlas/).

Figure 3. Tectonic setting of the northern boundary of the Caribbean plate from Early Eocene to Present-day times, modified from Leroy et al. (2000). See text for discussion.
B.R: Beata Ridge ; C. Sept. CF: Cauto Fault; CFZ: Camú Fault Zone; EPGFZ: Enriquillo-Plantain-Garden Fault Zone; H: Hispaniola block; J: Jamaica; NHDB: Northern Hispaniola Deformed Belt; NHFZ: Northern Hispaniola Fault Zone. OFZ: Oriente Fault Zone; SFZ:

Septentrional Fault Zone; SOFZ: Septentrional Oriente Fault Zone; WPD: Windward Passage Deep; WPS: Windward Passage Sill; YB: Yucatan Basin; TF: Trocha fault.

Figure 4. Overview of interpreted seismic units through the WPD and the WPS areas from Eocene to Present-day. A time calibration is proposed. Units 1, 3 and 4 were first named in the work of Calais & Mercier de Lépinay (1995) as B, A' and A, respectively. Unc.: unconformity.

Figure 5. Seismic profile covering the Windward Passage Deep (south) and part of the Windward Passage Sill (north). Unit 2 is perched and laterally discontinuous southward. The WPS high active reverse faults propagate upwards reaching the seafloor. Faults in red are upward spreading strands of wrench faults. Normal and thrust faults are, respectively, outline in violet and black colors. Inset 1: Location of the seismic line. Inset 2: Seismic line displayed with no vertical exaggeration according to the seafloor.

Figure 6. Seismic profile crossing the Windward Passage Deep (south) and Windward Passage Sill (north). In the Windward Passage Sill, sediments of unit 1 are deformed by older thrust faults. Black dashed lines are inferred faults based on the folded unconformities Uc1 and Uc3. Inset 1: Location of the seismic line.

Figure 7: Seismic profile crossing the Windward Passage Deep (south) and Windward Passage Sill (north). Wrench faults offset the Windward Passage Sill and developed a positive flower structure. The WPS high buildup-structure bordered by reverse faults indicates uplift along the Windward Passage Sill. See inset and Figure 2 for location of profile

Figure 8. Seismic profiles in the Windward Passage Sill with interpreted seismic units and its relative unconformities. Inset map shows seismic lines location.

Figure 9. Seismic profile across the Windward Passage Deep. Sets of reverse faults are identified on either edge of the basin. See inset and Figure 2 for profile location.

Figure 10. Seismic profile across the Windward Passage Deep. The unit 2 are uplifted in its northern border. Faults in red highlight the typical expression of the Septentrional–Oriente Fault zone (SOFZ) in the Windward Passage Deep. Pre-existing northern border fault firstly with a normal component and secondly with a reverse component is represented in violet. See inset and Figure 2 for location of profile.

Figure 11. Seismic profile across the Windward Passage Deep. Sets of reverse faults structural high on the southern edge of the basin. The unit 2 thickens toward the fault highlighting a syntectonic wedge related to a normal faulting. See inset and Figure 2 for profile location.

Figure 12. Two seismic profiles located in the Windward Passage Sill (see inset for location) with interpreted seismic units and its relative unconformities. (a) A narrow wrench fault deformation zone shifts acoustic basement and the sediment layers in the WPS central part. (b) The deformed area can be followed westward on parallel seismic lines. See inset and Figure 2 for profile location.

Figure 13. Four cross-sections across the Windward Passage area showing our summary schematic interpretation from the tectonic framework, as discerned from seismic images presented in this paper. Summary schematic interpretation of the tectonic framework across the Windward Passage, as discerned from seismic images presented in this paper. Inset map shows seismic lines location.

Figure 14. Sketches of the Windward Passage tectonic evolution in four main tectonic phases from Mid-late Eocene to Late-Pliocene to Present-day. Not to scale.

Figure 15. Isopach map of the unit 2 showing the 80km displacement of the Windward Passage Deep depocencer though east. Note that the bold reverse branches of SOFZ (north to the S2 segment) delimits well the unit 2 depocenter. These two fault strands probably accommodate part of the lateral relative motion during the left-lateral displacement of this unit.

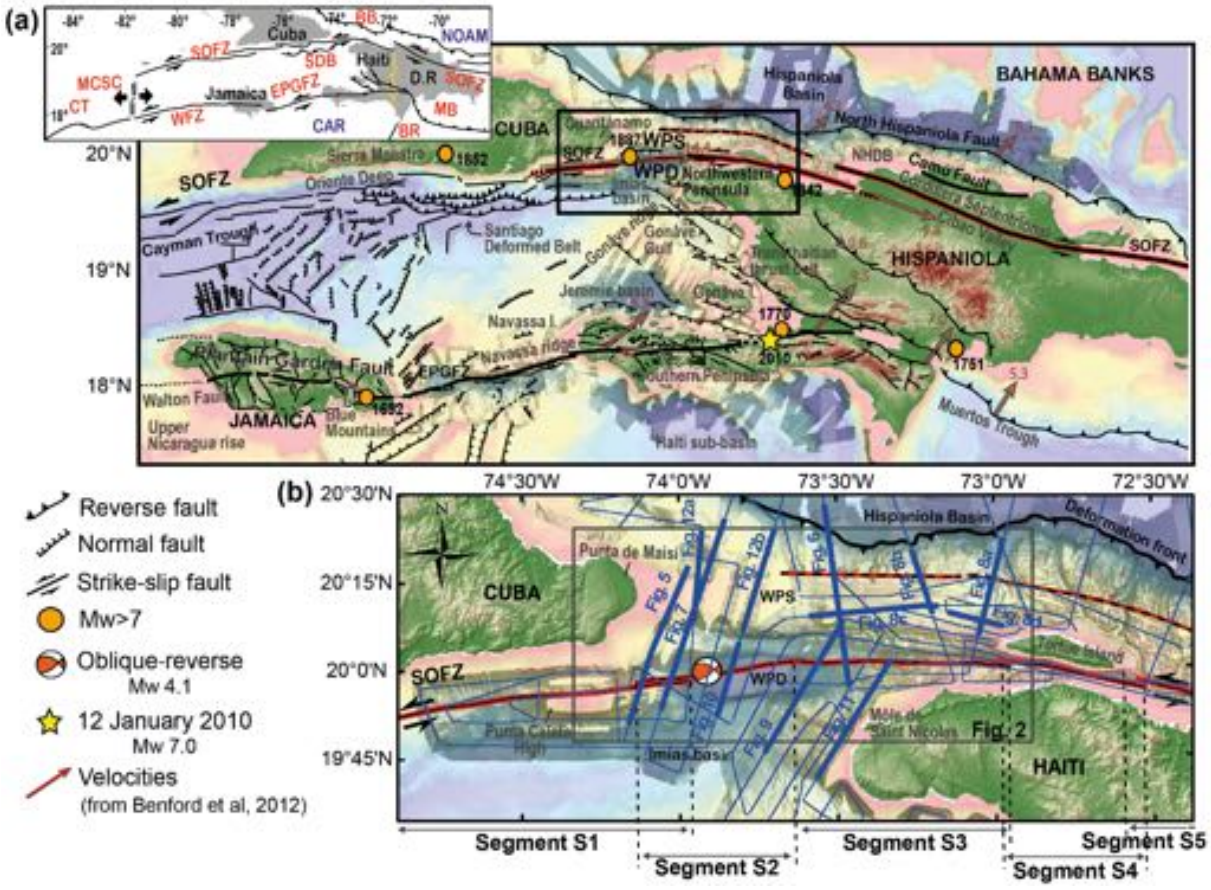
(a)
Cuba
Haiti
Jamaica
D.R
NOAM
SOFZ
SDB
MCSC
CT
WFZ
EPGFZ
CAR
BR
MB
SBR
CUBA
HISPANIOLA
BAHAMA BANKS
Hispaniola Basin
North Hispaniola Fault
Camu Fault
NHDB
WPS
WPD
Northwestern Peninsula
Guantanamo
Sierra Maestra
Oriente Deep
Cayman Trough
Santiago Deformed Belt
Gonâve Gulf
Gonâve ridge
Jeremie basin
Navassa I.
Navassa ridge
Walton Fault
Upper Nicaragua rise
JAMAICA
Blue Mountains
Muertos Trough
Haiti sub-basin
Northern Peninsula
Southern Peninsula
1770
2010
1751
1692
1842
5.3
20°N
19°N
18°N
74°30'W
74°0'W
73°30'W
73°0'W
72°30'W
(b)
20°30'N
20°15'N
20°0'N
19°45'N
Punta de Maisi
Punta Caleta High
Fig. 5
Fig. 7
Fig. 8c
Fig. 8a
Fig. 8b
Fig. 9
Fig. 10
Fig. 11
Fig. 12a
Fig. 12b
Fig. 6
Fig. 3a
Fig. 3b
Fig. 2
Zoetle Island
Deformation front
Segment S1
Segment S2
Segment S3
Segment S4
Segment S5
Reverse fault
Normal fault
Strike-slip fault
Mw>7
Oblique-reverse
Mw 4.1
12 January 2010
Mw 7.0
Velocities
(from Benford et al, 2012)

Figure 1

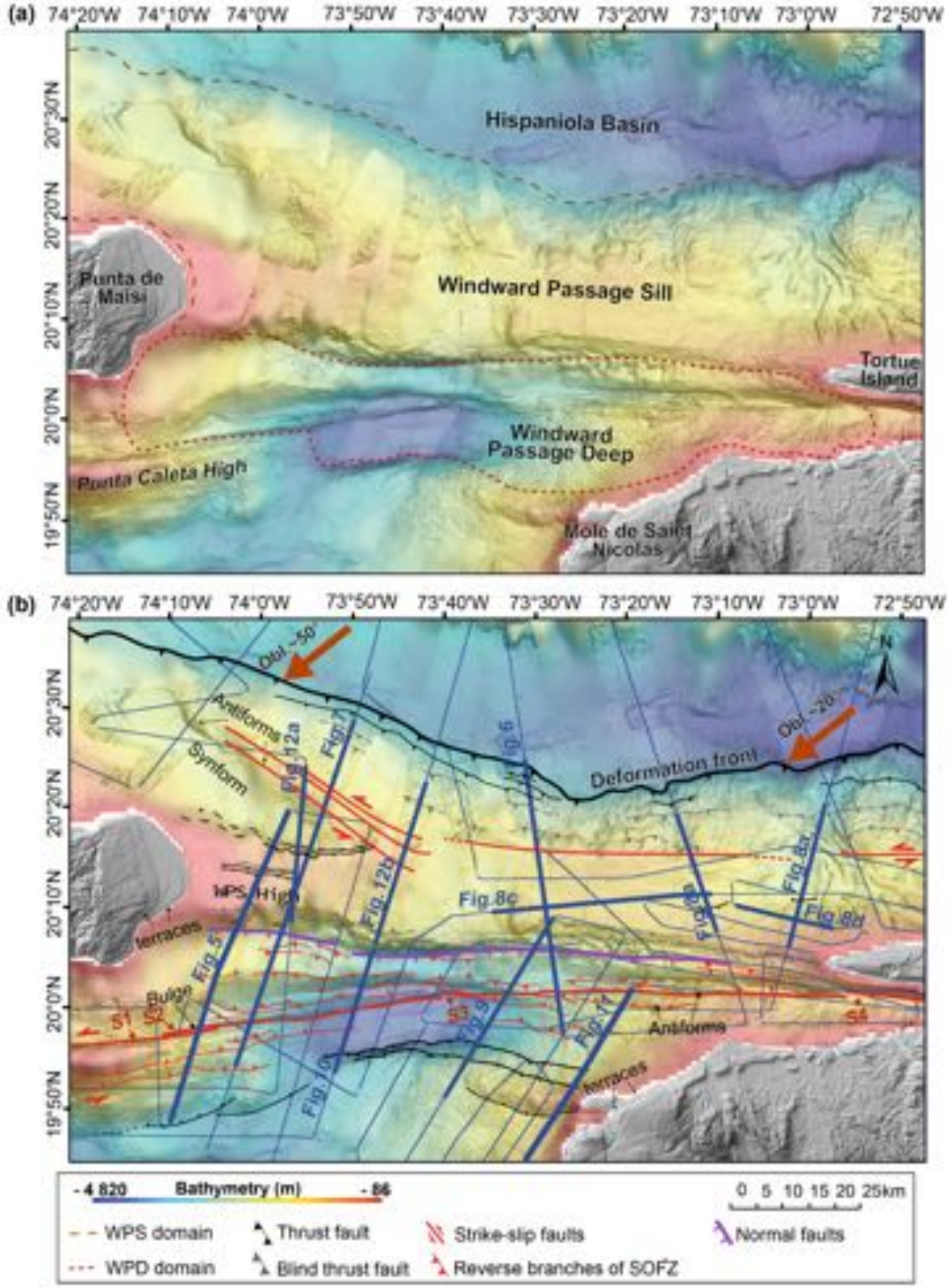
(a)
74°20'W
74°10'W
74°0'W
73°50'W
73°40'W
73°30'W
73°20'W
73°10'W
73°0'W
72°50'W
20°30'N
20°20'N
20°10'N
20°0'N
19°50'N
Hispaniola Basin
Punta de Maisi
Windward Passage Sill
Tortue Island
Windward Passage Deep
Punta Caleta High
Mole de Saint Nicolas
(b)
Obl. ~50°
Obl. ~20°
N
Antiforms
Synform
Fig.12a
Fig.7
Fig.6
Deformation front
Fig.12b
Fig.8c
Fig.8a
Fig.8b
WPS High
Terraces
Fig.5
Bulge
S1
S2
S3
S4
Fig.9
Fig.11
Antiforms
Terraces
- 4 820
Bathymetry (m)
- 86
0 5 10 15 20 25km
WPS domain
WPD domain
Thrust fault
Blind thrust fault
Strike-slip faults
Reverse branches of SOFZ
Normal faults

Figure 2.

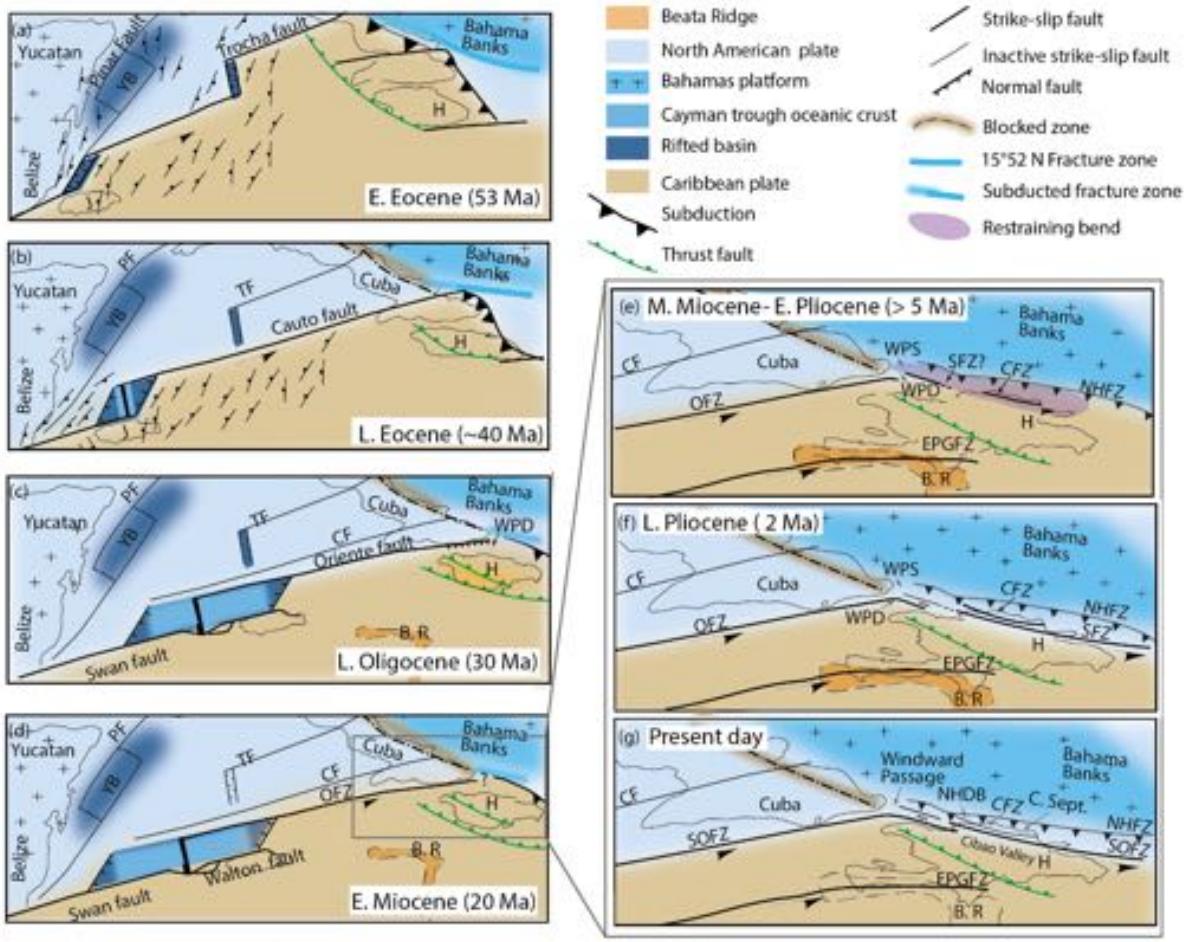
(a)
Yucatan
Polochic fault
Trocha fault
YB
Belize
Bahama Banks
H
E. Eocene (53 Ma)
(b)
PF
Yucatan
YB
TF
Cauto fault
Cuba
Bahama Banks
Belize
H
L. Eocene (~40 Ma)
(c)
PF
Yucatan
YB
TF
CF
Oriente fault
Cuba
Bahama Banks
WPD
H
B. R
Belize
Swan fault
L. Oligocene (30 Ma)
(d)
PF
Yucatan
YB
TF
CF
OFZ
Cuba
Bahama Banks
H
B. R
Belize
Walton fault
Swan fault
E. Miocene (20 Ma)
Beata Ridge
North American plate
Bahamas platform
Cayman trough oceanic crust
Rifted basin
Caribbean plate
Subduction
Thrust fault
Strike-slip fault
Inactive strike-slip fault
Normal fault
Blocked zone
15°52 N Fracture zone
Subducted fracture zone
Restraining bend
(e) M. Miocene - E. Pliocene (> 5 Ma)
Bahama Banks
CF
Cuba
WPS
SFZ?
CFZ
NHFZ
OFZ
WPD
H
EPGFZ
B. R
(f) L. Pliocene (2 Ma)
Bahama Banks
CF
Cuba
WPS
CFZ
NHFZ
OFZ
WPD
SFZ
H
EPGFZ
B. R
(g) Present day
Windward Passage
Bahama Banks
CF
Cuba
NHDB
CFZ
C. Sept.
NHFZ
SOFZ
SOFZ
Cibao Valley
H
EPGFZ
B. R

Figure 3.

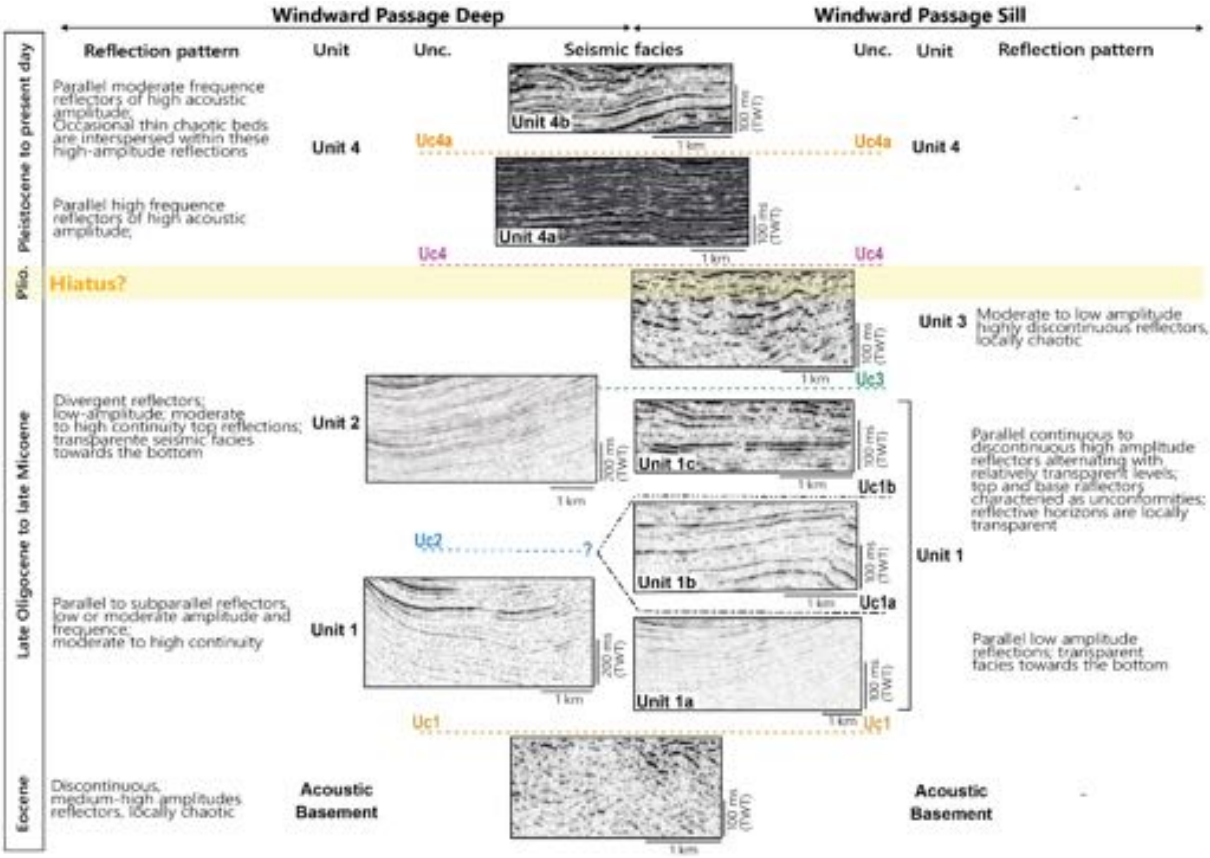
Windward Passage Deep
Windward Passage Sill
Reflection pattern
Unit
Unc.
Seismic facies
Unc.
Unit
Reflection pattern
Pleistocene to present day
Plio.
Late Oligocene to late Miocene
Eocene
Parallel moderate frequence reflectors of high acoustic amplitude; Occasional thin chaotic beds are interspersed within these high-amplitude reflections
Unit 4
Uc4a
Unit 4b
Unit 4
Parallel high frequence reflectors of high acoustic amplitude;
Unit 4a
Uc4
Uc4
Hiatus?
Unit 3
Moderate to low amplitude highly discontinuous reflectors, locally chaotic
Uc3
Divergent reflectors; low-amplitude; moderate to high continuity top reflections; transparente seismic facies towards the bottom
Unit 2
Unit 1c
Uc1b
Parallel continuous to discontinuous high amplitude reflectors alternating with relatively transparent levels; top and base reflectors characterised as unconformities; reflective horizons are locally transparent
Uc2
?
Unit 1b
Unit 1
Uc1a
Parallel to subparallel reflectors, low or moderate amplitude and frequence; moderate to high continuity
Unit 1
Unit 1a
Parallel low amplitude reflections; transparent facies towards the bottom
Uc1
Uc1
Discontinuous, medium-high amplitudes reflectors, locally chaotic
Acoustic Basement
Acoustic Basement
1 km
100 ms (TWT)
200 ms (TWT)
300 ms (TWT)

Figure 4.

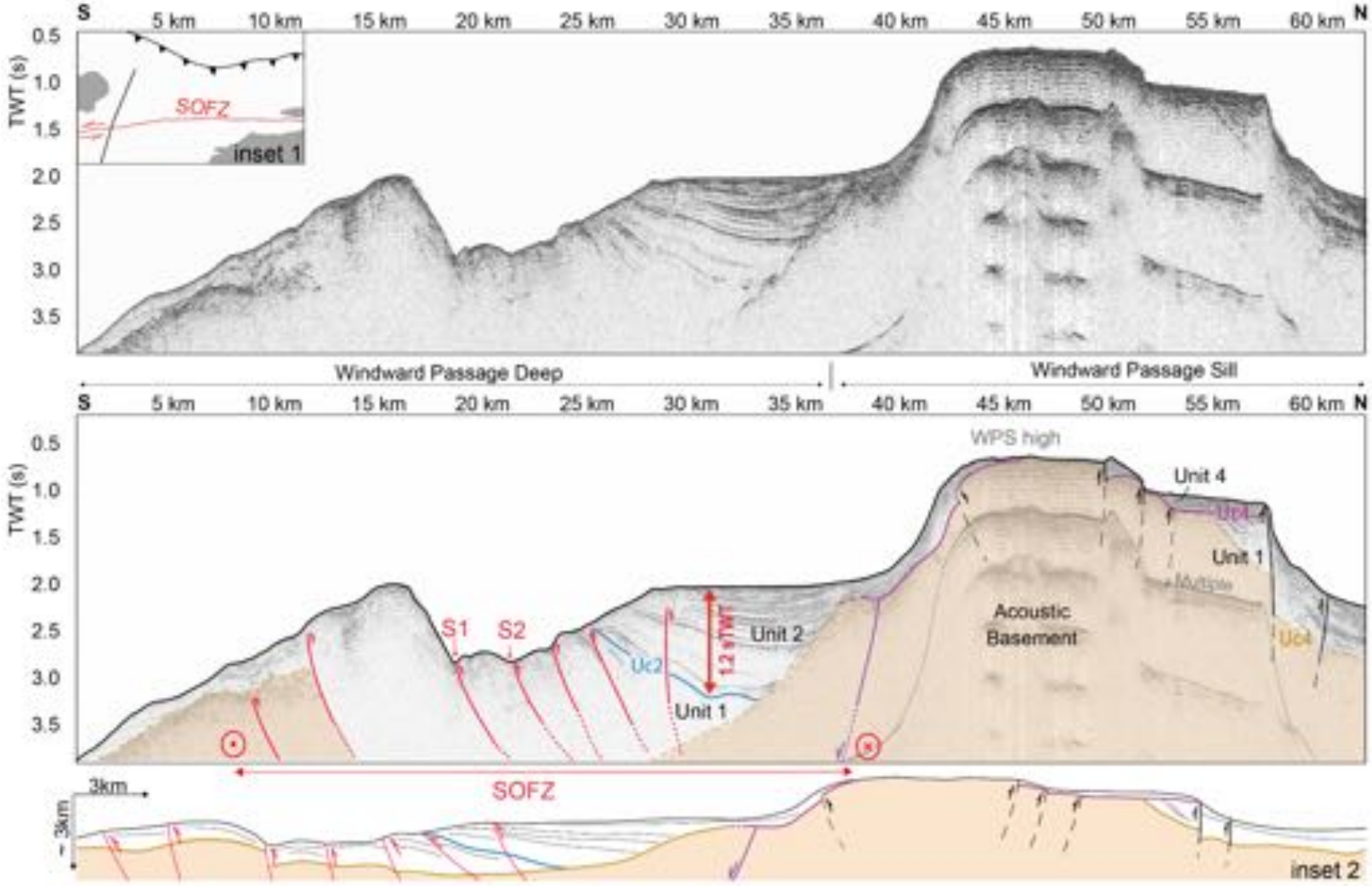
S
5 km
10 km
15 km
20 km
25 km
30 km
35 km
40 km
45 km
50 km
55 km
60 km
N
TWT (s)
0.5
1.0
1.5
2.0
2.5
3.0
3.5
SOFZ
inset 1
Windward Passage Deep
Windward Passage Sill
WPS high
Unit 4
Unit 1
Acoustic
Basement
S1
S2
Unit 2
1.2 s TWT
Uc2
Unit 1
SOFZ
3km
3km
inset 2

Figure 5

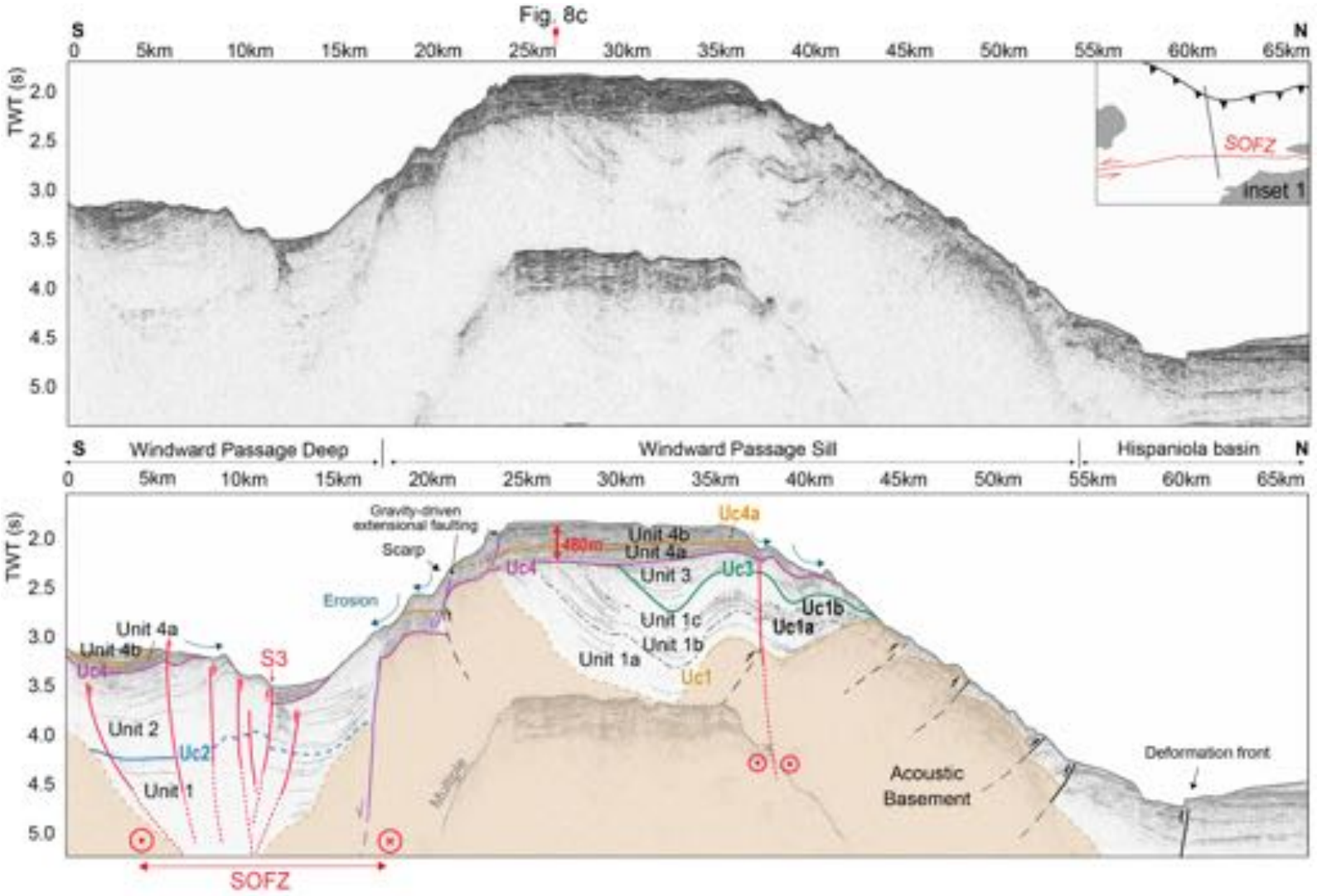
Fig. 8c
S
N
0
5km
10km
15km
20km
25km
30km
35km
40km
45km
50km
55km
60km
65km
TWT (s)
2.0
2.5
3.0
3.5
4.0
4.5
5.0
SOFZ
Inset 1
Windward Passage Deep
Windward Passage Sill
Hispaniola basin
Gravity-driven extensional faulting
Scarp
Erosion
480m
Unit 4b
Unit 4a
Unit 3
Unit 1c
Unit 1b
Unit 1a
Uc4a
Uc4
Uc3
Uc1b
Uc1a
Uc1
S3
Unit 2
Uc2
Unit 1
Acoustic Basement
Deformation front
SOFZ

Figure 6

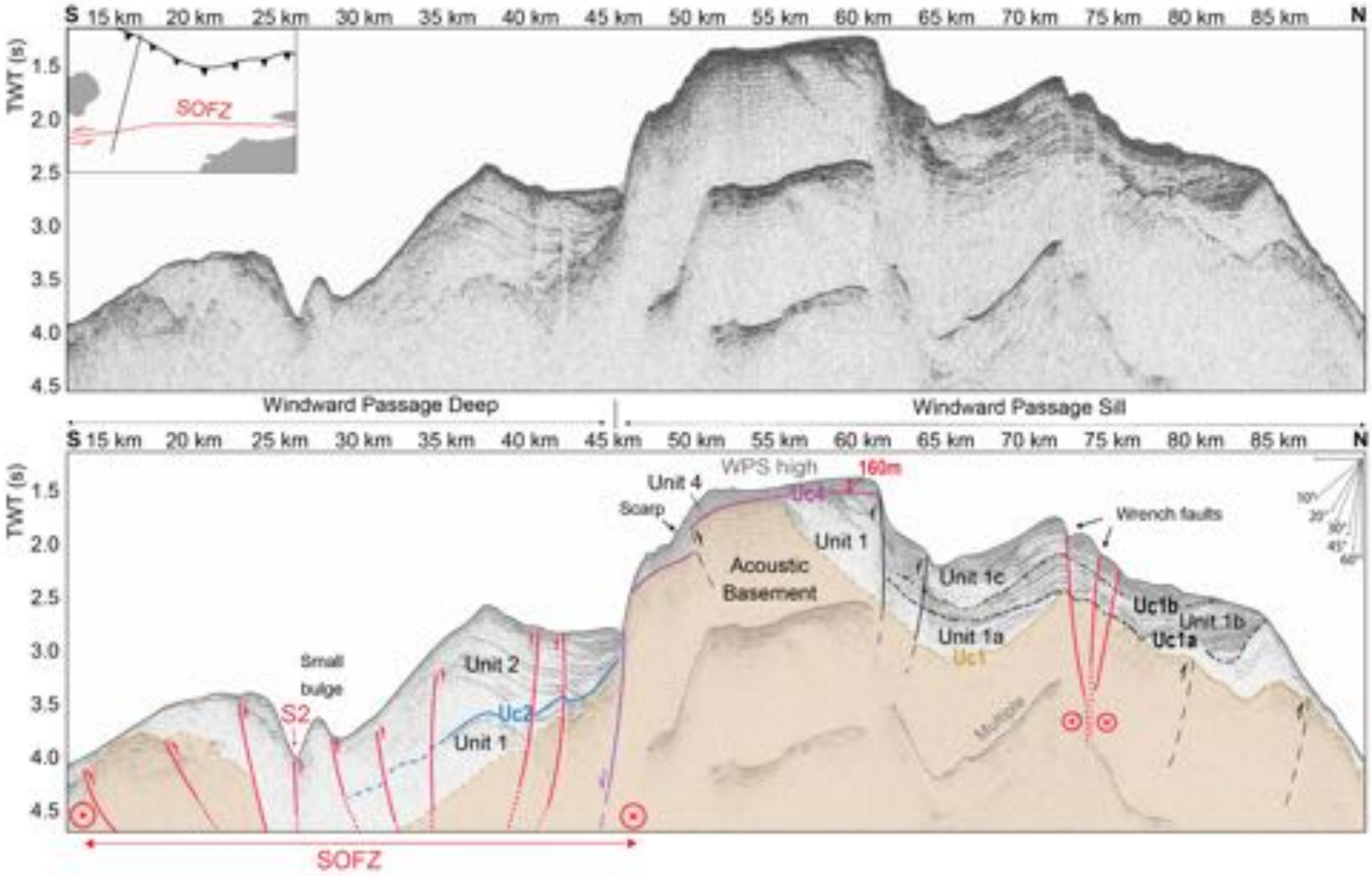
S
15 km
20 km
25 km
30 km
35 km
40 km
45 km
50 km
55 km
60 km
65 km
70 km
75 km
80 km
85 km
N
TWT (s)
1.5
2.0
2.5
3.0
3.5
4.0
4.5
SOFZ
Windward Passage Deep
Windward Passage Sill
WPS high
160m
Unit 4
Uc4
Scarp
Unit 1
Acoustic
Basement
Unit 1c
Wrench faults
Uc1b
Unit 1b
Uc1a
Unit 1a
Uc1
Small
bulge
S2
Unit 2
Uc2
Unit 1
Multiple
SOFZ

Figure 7

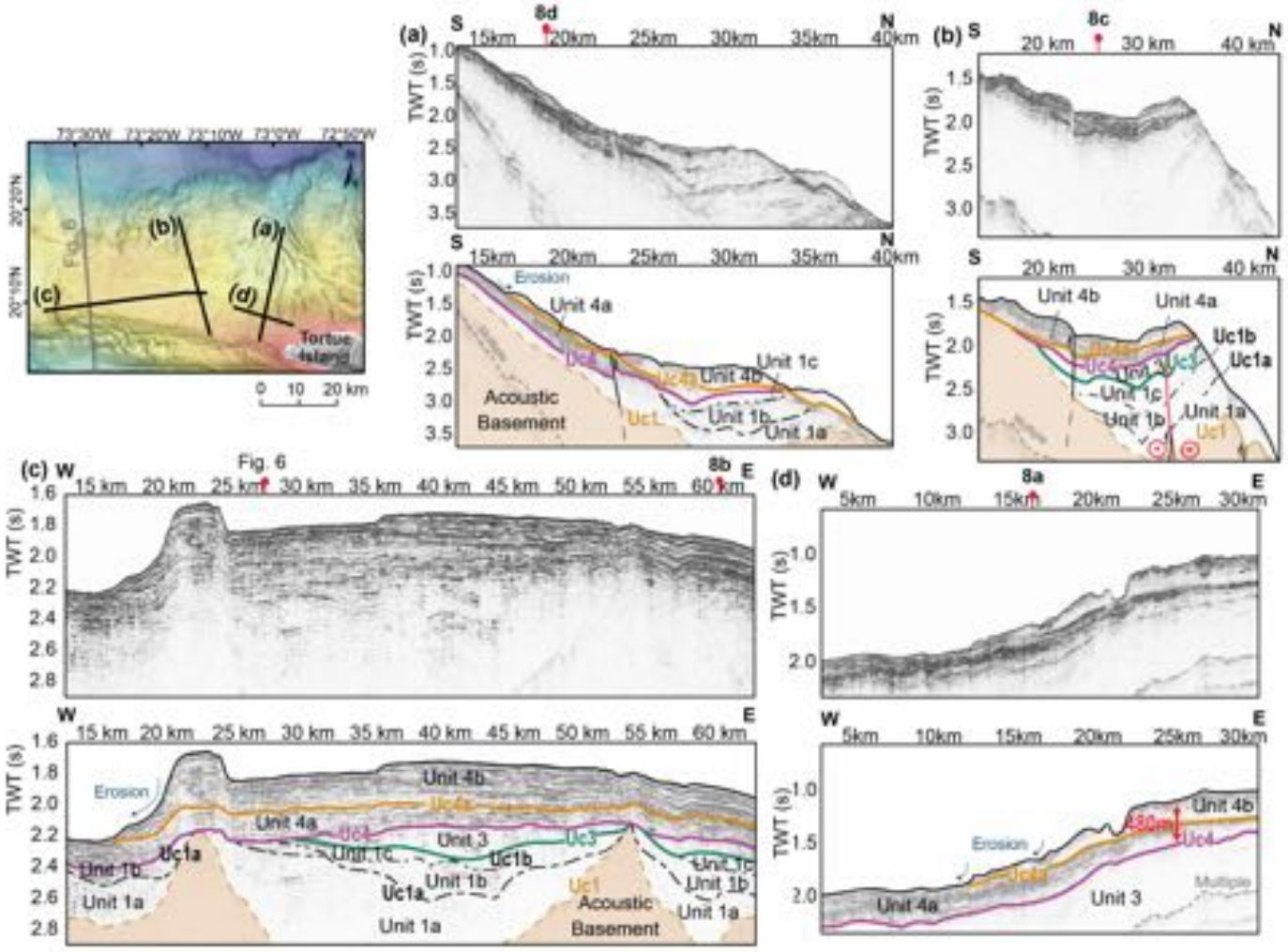
(a)
(b)
(c)
(d)
Fig. 6
Tortue Island
0 10 20 km
8d
8c
8b
8a
S
N
W
E
TWT (s)
Erosion
Unit 4a
Unit 4b
Unit 1c
Unit 1b
Unit 1a
Acoustic Basement
Uc1
Uc1a
Uc1b
Uc3
Uc4
Unit 3
Multiple

Figure 8

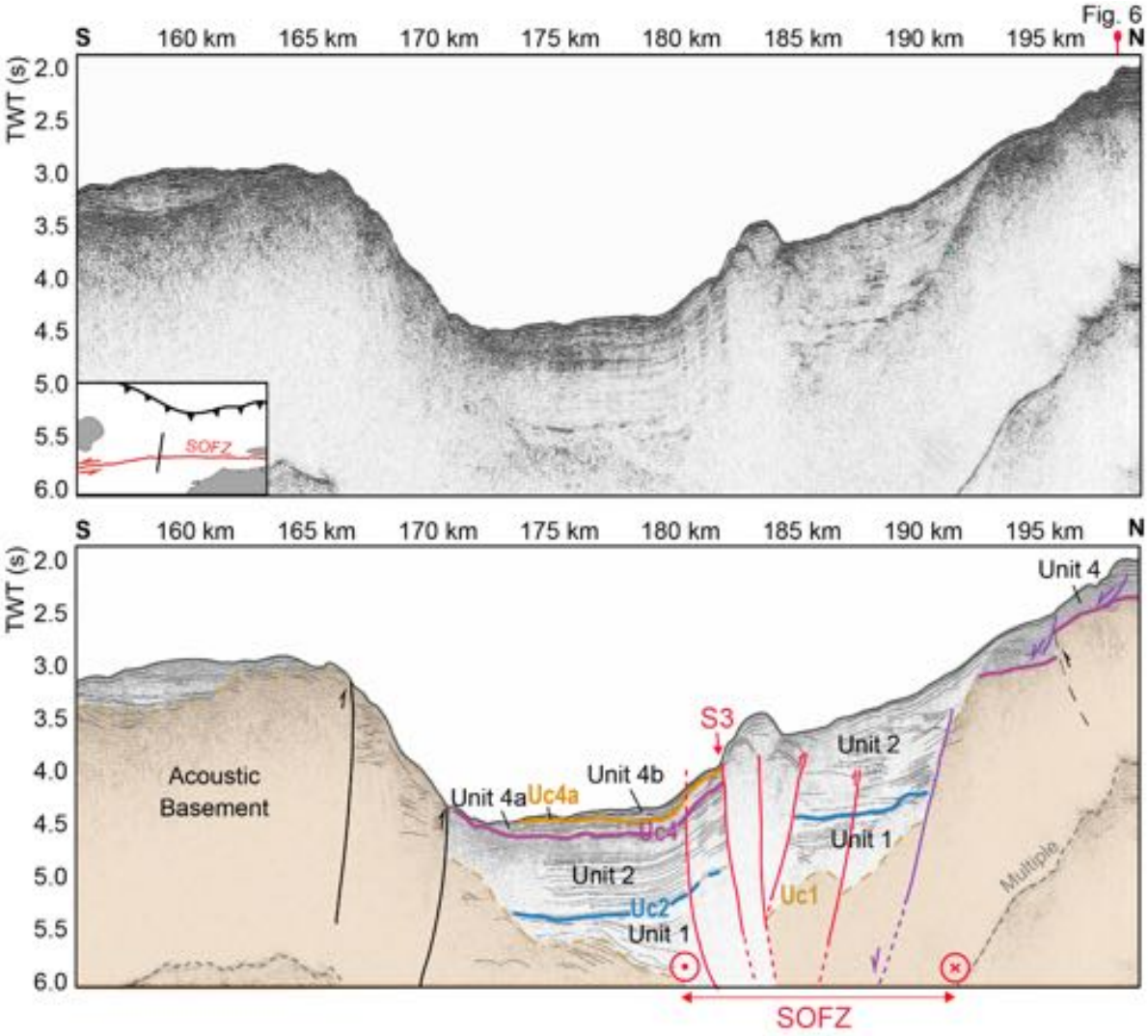
Fig. 6
S
160 km
165 km
170 km
175 km
180 km
185 km
190 km
195 km
N
TWT (s)
2.0
2.5
3.0
3.5
4.0
4.5
5.0
5.5
6.0
SOFZ
Acoustic Basement
Unit 4a
Uc4a
Unit 4b
Uc4
Unit 2
Uc2
Unit 1
S3
Unit 2
Unit 1
Uc1
Unit 4
Multiple
SOFZ

Figure 9

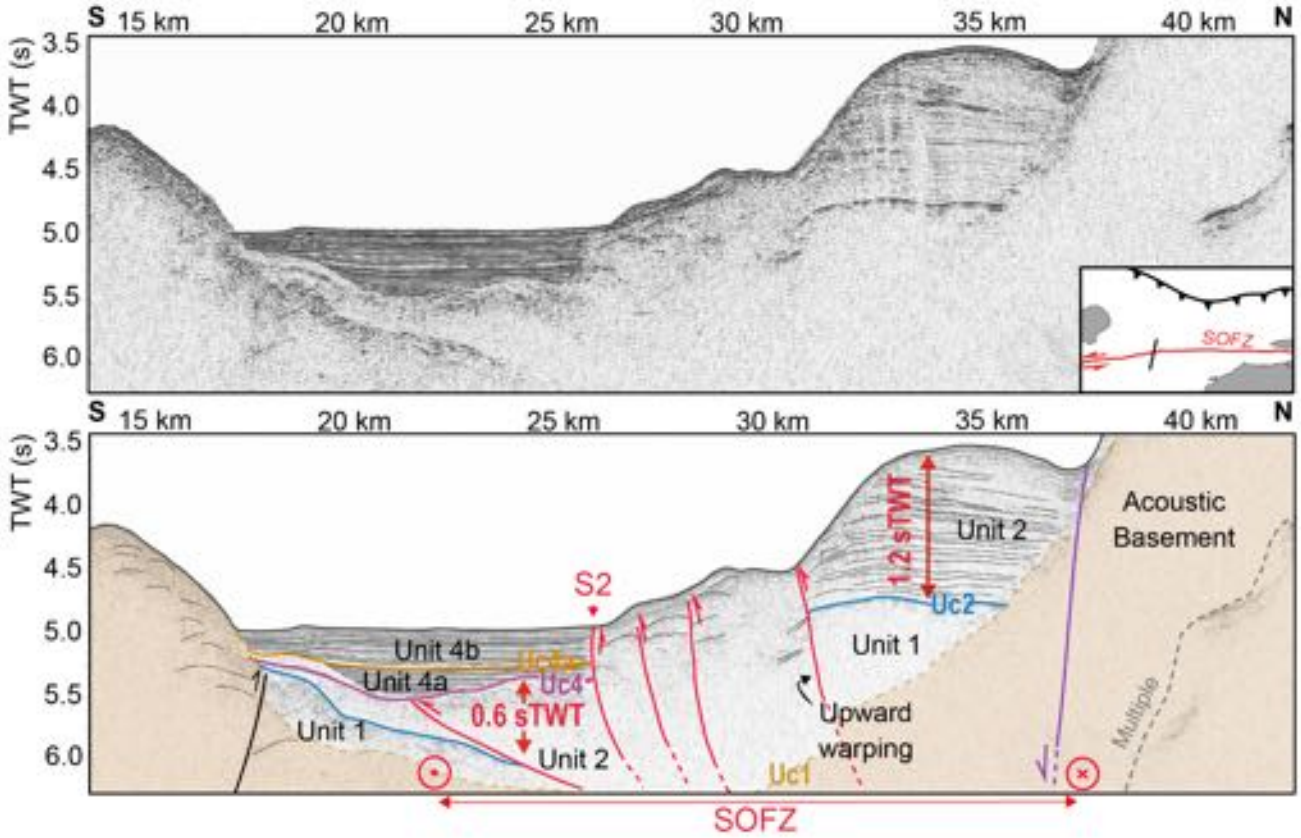
S
15 km
20 km
25 km
30 km
35 km
40 km
N
TWT (s)
3.5
4.0
4.5
5.0
5.5
6.0
SOFZ
Unit 4b
Unit 4a
Uc4
0.6 sTWT
Unit 1
Unit 2
S2
Uc1
1.2 sTWT
Unit 2
Uc2
Unit 1
Upward warping
Acoustic Basement
Multiple
SOFZ

Figure 10

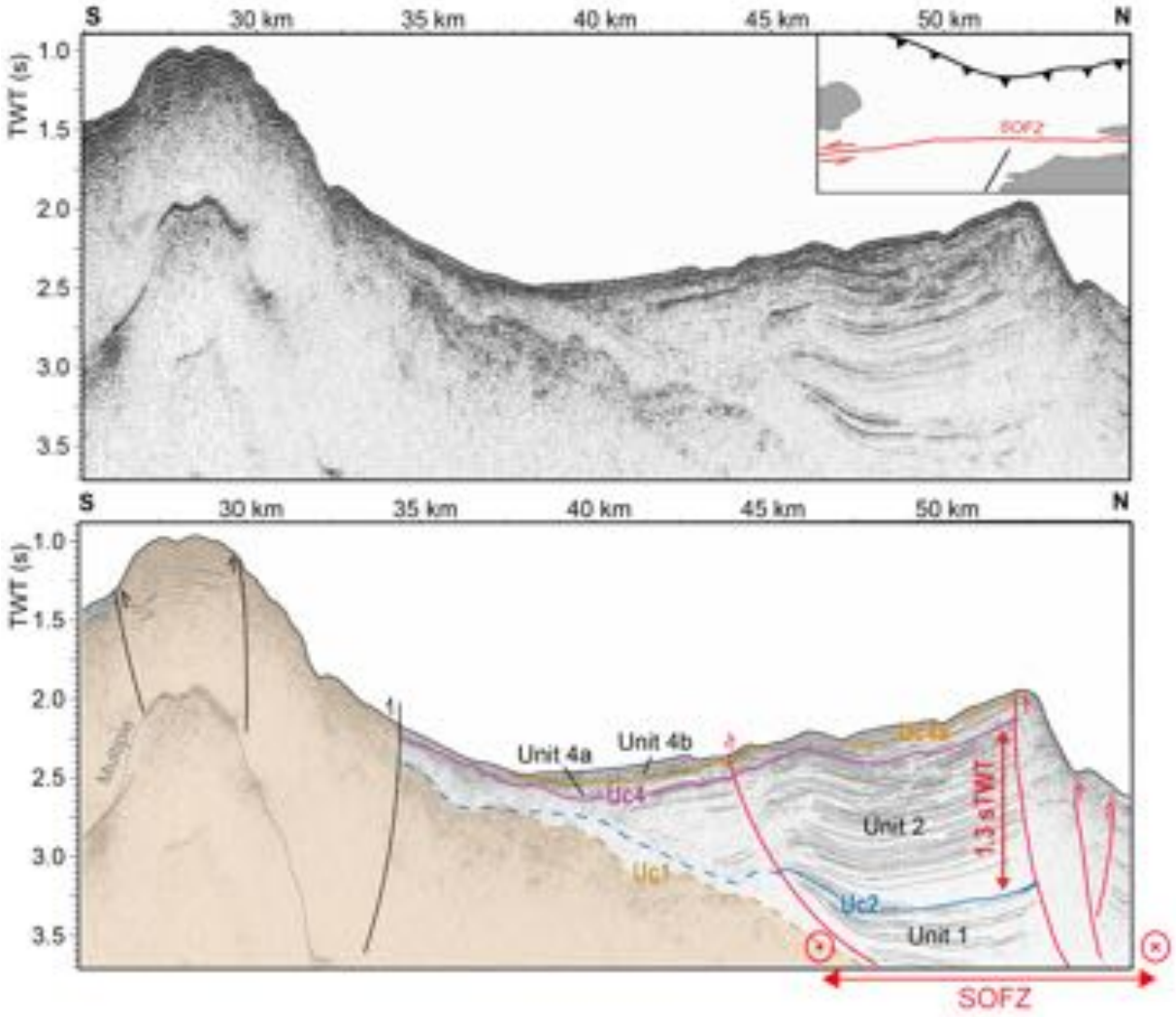
S
30 km
35 km
40 km
45 km
50 km
N
TWT (s)
1.0
1.5
2.0
2.5
3.0
3.5
SOFZ
Unit 4a
Unit 4b
Uc4
Unit 2
1.3 s TWT
Uc1
Uc2
Unit 1
SOFZ

Figure 11

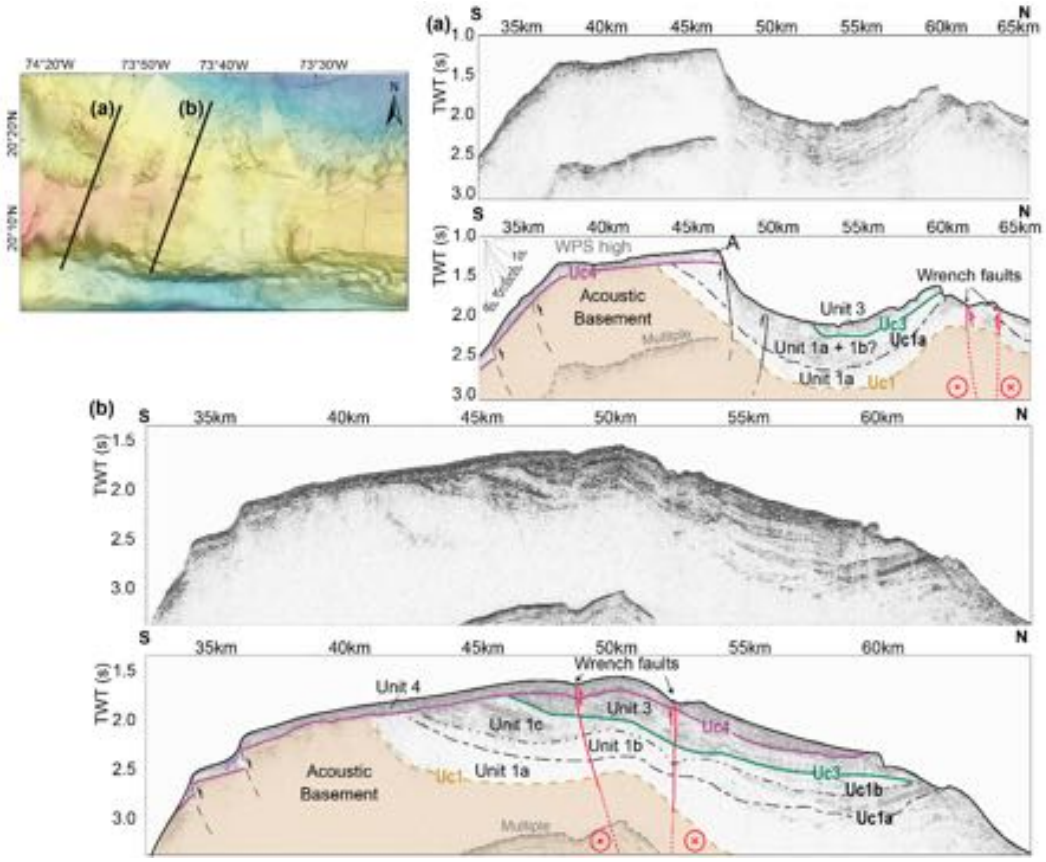
74°20'W
73°50'W
73°40'W
73°30'W
20°20'N
20°10'N
(a)
(b)
N
(a)
S
N
35km
40km
45km
50km
55km
60km
65km
TWT (s)
1.0
1.5
2.0
2.5
3.0
WPS high
A
Uc4
Acoustic
Basement
Unit 3
Uc3
Uc1a
Unit 1a + 1b?
Unit 1a
Uc1
Wrench faults
Multiple
(b)
Unit 4
Unit 1c
Unit 1b
Unit 1a
Uc1
Uc4
Uc3
Uc1b
Uc1a

Figure 12

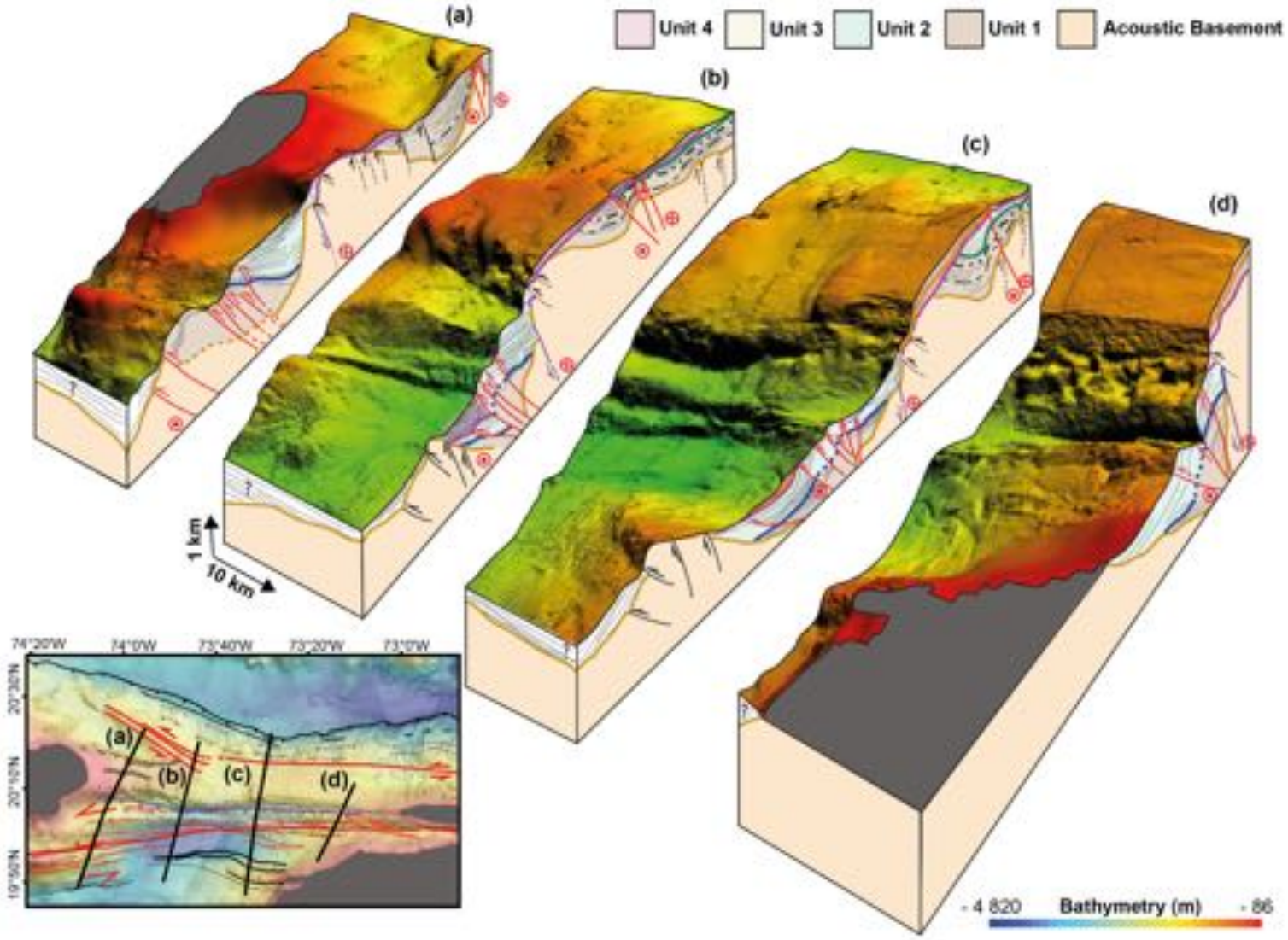
(a)
(b)
(c)
(d)
Unit 4
Unit 3
Unit 2
Unit 1
Acoustic Basement
1 km
10 km
74°20'W
74°0'W
73°40'W
73°20'W
73°0'W
20°30'N
20°10'N
19°50'N
- 4 820
Bathymetry (m)
- 86

Figure 13

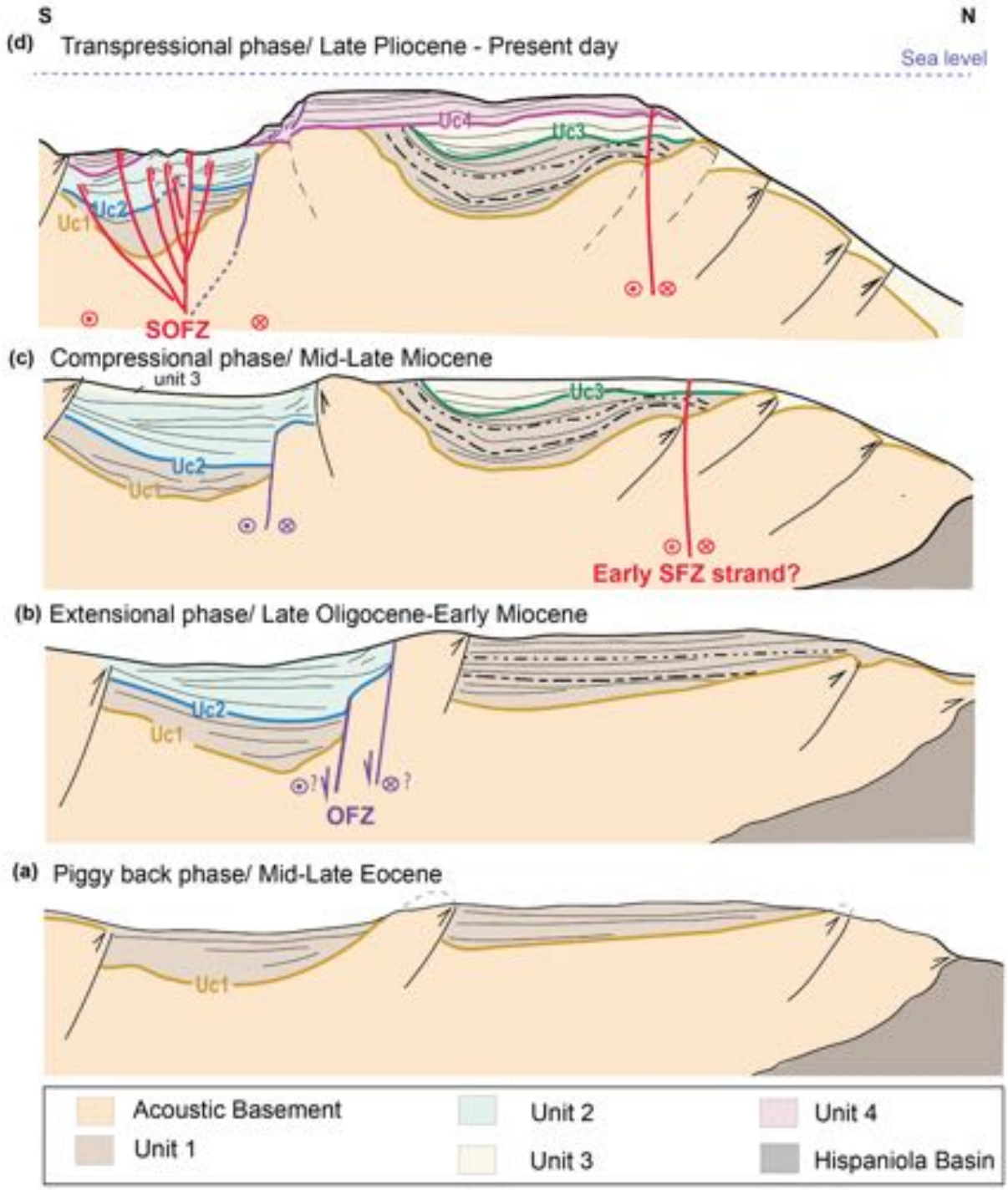
S
N
(d) Transpressional phase/ Late Pliocene - Present day
Sea level
Uc4
Uc3
Uc2
Uc1
SOFZ
(c) Compressional phase/ Mid-Late Miocene
unit 3
Uc3
Uc2
Uc1
Early SFZ strand?
(b) Extensional phase/ Late Oligocene-Early Miocene
Uc2
Uc1
OFZ
(a) Piggy back phase/ Mid-Late Eocene
Uc1
Acoustic Basement
Unit 1
Unit 2
Unit 3
Unit 4
Hispaniola Basin

Figure 14

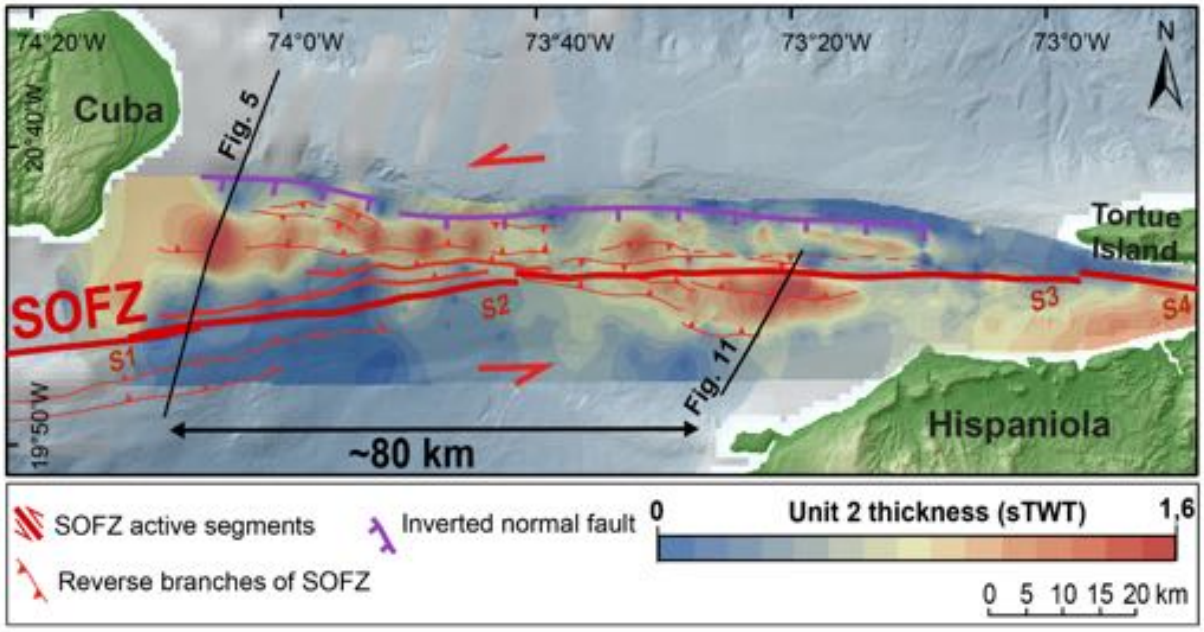
74°20'W
74°0'W
73°40'W
73°20'W
73°0'W
N
20°40'W
19°50'W
Cuba
Fig. 5
Fig. 11
SOFZ
S1
S2
S3
S4
Tortue Island
Hispaniola
~80 km
SOFZ active segments
Inverted normal fault
Reverse branches of SOFZ
0
Unit 2 thickness (sTWT)
1,6
0 5 10 15 20 km

Figure 15